telecom

MDPI

Article

Power-Efficient Ultra-Reliable Communication in Rayleigh–Rayleigh Fading Environment Using ARQ-I and CC-HARQ

Supun Fernando [1,*], Uditha Wijewardhana [2] and Nishan Dharmaweera [2]

[1] Department of Electrical, Electronic and Telecommunication Engineering, General Sir John Kotelawala Defence University, Ratmalana 10390, Sri Lanka

[2] Department of Electrical and Electronic Engineering, University of Sri Jayewardenepura, Nugegoda 10250, Sri Lanka; uditha@sjp.ac.lk (U.W.); nishanmd@sjp.ac.lk (N.D.)

* Correspondence: supunfernando@kdu.ac.lk

Abstract

We propose optimal power allocation for a transmitter that operates with either the ARQ-I or CC-HARQ protocol in an interference-limited environment where both the desired and interfering signals experience Rayleigh fading, forming an analytically tractable non-line-of-sight scenario, to achieve ultra-reliable communication with minimal power. We formulate the power allocation problem as a minimization of the average retransmit power under a given target outage probability for both retransmission schemes. Using the Karush–Kuhn–Tucker method, we derive protocol-specific equations solved numerically for retransmit powers. Unlike prior interference-limited numerical studies and noise-limited closed-form results, we derive closed-form analytical solutions for optimal retransmit power expressions for ARQ-I and CC-HARQ in a Rayleigh–Rayleigh interference-limited environment for two retransmissions, which act as computationally efficient benchmarks for real-time ultra-reliable applications and establish a baseline for extending to more general fading environments. This constitutes the primary contribution of this work. We show through simulations that the proposed schemes achieve significant power savings compared to conventional open-loop transmission, particularly in the ultra-reliable region. Benchmarking against prior Rician–Rayleigh results shows that, as expected, the Rayleigh–Rayleigh case requires higher power because it lacks the line-of-sight component that improves reliability, while confirming that CC-HARQ consistently outperforms ARQ-I in power efficiency.

Keywords: ultra-reliabile communication; Rayleigh fading; power optimization; ARQ-I; CC-HARQ

Check for updates

Academic Editors: Adamantia Stamou, Artur Hecker, Marvin Sanchez and Luis Miguel Contreras-Murillo

Received: 29 December 2025
Revised: 10 March 2026
Accepted: 12 March 2026
Published: 1 September 2026

1. Introduction

One of the main aspects in mobile communications is to provide a reliable connection for users. The reliability of a connection is lost by the outages which are caused when the signal-to-noise ratio (SNR) at the receiver goes below a pre-defined threshold value [1]. The reason for the reduction in SNR below this value is fading. Further, due to the scarcity of the spectrum, the same frequency band is used in nearby cells. This results in co-channel interferers in cellular networks [2], which also cause outages. Systems in which the dominant cause of outages is interferers are called interference-limited systems. In such systems, outages are caused when the signal-to-interference ratio (SIR) at the receiver goes below a pre-defined threshold value, which is called the signal-to-interference protection ratio (SIPR) [3].

Amidst all these difficulties, 5G introduced several operating modes, including the Ultra-Reliable and Low-Latency Communication (URLLC) mode [4]. This communication mode was further enhanced in 6G, and ref. [5] states that it is one of the most challenging objectives in 6G networks. Typically, for mobile communication systems, URLLC requires a reliability of more than 99.999% and a latency of less than 10 ms [5,6]. URLLC is mostly required in reliable-critical and mission-critical applications such as 6G-enabled Internet of Things [7], where uninterrupted and robust exchange of data between universally connected devices is of utmost importance [8–10]. Since the electromagnetic energy used in data transmission is obtained by converting electrical energy, if used with efficient power allocation, it could reduce the power usage, making the communication system reliable while being energy-efficient.

While URLLC requires both ultra-high reliability and low latency, these requirements are closely linked through the allowable number of retransmissions. In this work, we derive optimal power allocation solutions for a general maximum number of transmissions M, thereby addressing the ultra-reliability aspect. However, the low-latency requirement in practical URLLC systems inherently limits the maximum allowable retransmissions. Prior studies [11–13] indicate that, depending on system parameters and protocols, the number of retransmissions is typically $M \leq 4$ to meet latency constraints. Determining the maximum feasible number of retransmissions for a given protocol and fading environment without violating latency requirements is itself a separate system-level design problem. Therefore, this work focuses on deriving optimal power allocations for retransmissions, which is the Ultra-Reliable Communication (URC) part of the URLLC, which provides a fundamental reliability–power tradeoff framework applicable to latency-constrained URLLC operation.

A simple way to achieve URC is to consider the outage expression for the scenario and boost the transmit power to reduce the required outage to 0.00001. However, such open-loop transmission systems have been mentioned in [11,14] as power-inefficient. Thus, retransmission systems that employ error control methods are used extensively in practice. Error control methods reduce outages to obtain high reliabilities by combining error detection with retransmission on request [15]. The two basic categories of error control schemes are Automatic Repeat Request (ARQ) schemes and Forward Error Correction schemes. When these two schemes are combined, this is called the Hybrid Automatic Repeat Request (HARQ) scheme [15,16].

1.1. Motivation

Achieving URC will be one of several goals in next-generation mobile networks [4]. On the other hand, the world is moving towards sustainability and green concepts to bring about energy-efficient technologies. Thus, systems above 5G have adopted energy efficiency as one of their evaluation metrics [17].

As mentioned above, a simple and elegant way to achieve URC will be to use a communication system that uses an open-loop transmission scheme. To put it simply, the system achieves high reliabilities by increasing the transmit power. However, this method consumes a lot of power, as mentioned in [14,18,19], which will also be evident in our simulations. Therefore, this will violate the aforementioned energy-efficient criterion of next-generation networks.

Earlier work in this area such as [11–14,18,20] has shown that, by using retransmission schemes, the overall power requirement could be reduced to lower values, thus achieving higher power savings compared to the open-loop setup. Thus, we utilize communication systems that use retransmission schemes that employ error control methods to achieve high reliabilities. Since both ARQ and HARQ schemes are widely adopted in LTE-related systems, we assume the error control methods of the retransmission system to either be Type-I ARQ or Chase Combining HARQ (CC-HARQ). We see that by utilizing our power allocation schemes for the transmitters, a vast number of communication systems that work on these two protocols will achieve URC using the minimum amount of power, thereby adhering to the evaluation metrics for energy efficiency.

1.2. Related Work

1.2.1. ARQ-I

The use of the ARQ-I protocol to enhance system performance for achieving URC is discussed in [21]. This study introduces a new data transmission approach based on spatial diversity with ARQ-I to improve transmission reliability. An opportunistic transmission framework for a secondary user within the interweave model in the finite blocklength regime is explored in [22]. This framework defines access probabilities and transmission power to meet target error constraints, thereby ensuring ultra-reliability while minimizing transmit power. A power allocation strategy aimed at minimizing outage probability is presented in [23]. This approach also employs the ARQ protocol, even though the number of retransmissions is capped at two. However, this method does not meet the low outage probabilities necessary for URC. In [11], closed-form expressions for retransmit powers are derived for any number of retransmissions by solving a power allocation problem formulated to minimize the average retransmit power. All these works have considered the transmitter situated in a Rayleigh faded environment, without interference signals. An interference-limited ARQ-I system is discussed in [20], where the desired signal is Rician faded and the interferer signal is Rayleigh faded. This work derives a set of equations that can be numerically solved to determine the retransmit powers for any number of ARQ-I retransmissions.

1.2.2. CC-HARQ

An energy-efficient adaptive power allocation strategy for three incremental multiple-input–multiple-output systems utilizing CC-HARQ is introduced in [24], where the authors frame the problem as a geometric programming problem aimed at reducing the outage probability, providing closed-form solutions. However, it does not handle the issue of minimizing the power consumption. In a similar manner, ref. [25] offers a closed-form approximation for the outage probability of a system which uses the CC-HARQ protocol, again formulating the problem as a geometric programming problem. In the works of [12,14], the authors derive closed-form solutions to obtain CC-HARQ retransmit power values to achieve URC regardless of the number of retransmissions. While various methods have been proposed in the previously mentioned studies to achieve power-efficient ultra-reliability using the CC-HARQ protocol, they have all assumed Rayleigh fading environments without accounting for the presence of co-channel interferers. However, ref. [13] considers an interference-limited system, where the desired signal is Rician faded, while the interference signal is Rayleigh faded. In this work, the authors derive a set of equations which can be numerically solved to obtain the retransmit powers for any number of CC-HARQ retransmissions.

Recent works have explored various advanced techniques to enhance reliability, security, and latency performance in next-generation wireless systems. For example, hybrid active–passive reconfigurable intelligent surfaces (RISs) have been proposed to strengthen secure transmission by dynamically controlling reflected signals against eavesdropping and jamming attacks [26]. Learning-based approaches have also gained attention, including lightweight deep neural architectures for efficient temporal modeling [27] and deep reinforcement learning (DRL) frameworks for URLLC optimization [28]. From a theoretical perspective, closed-form performance bounds for delay violation probability under semantic communication paradigms have been derived using stochastic network calculus [29], while edge intelligence architectures leveraging mobile edge computing have been proposed to jointly satisfy reliability and latency requirements in emerging applications such as the industrial metaverse [30]. These studies highlight the growing emphasis on URLLC through diverse paradigms, motivating further analytical investigation of power-efficient retransmission strategies in interference-limited fading environments.

1.3. Unaddressed Issue

While much of the existing literature discussed above on ARQ-I and CC-HARQ protocols has provided valuable means to achieve URC in wireless networks, most of these studies have focused on Rayleigh fading environments without considering the presence of co-channel interference. This simplification overlooks the practical complexities encountered in real-world communication systems, where interference from other coexisting signals plays a significant role in system performance [31].

Works which have addressed interference-limited environments [13,20] have discussed systems with the desired signal undergoing Rician fading, while the interfering signal undergoes Rayleigh fading. While fading models such as Rician and Nakagami-m provide a more general representation of wireless channels, incorporating them into power minimization frameworks typically results in highly non-linear formulations that can only be solved numerically. In contrast, our work focuses on the Rayleigh–Rayleigh fading environment, which enables the derivation of closed-form analytical solutions for the optimal power allocation for the case of $M = 2$. This analytical tractability is particularly valuable for URC, where fast resource allocation decisions must be made under strict latency constraints.

Our previous work in [18] derived closed-form retransmit power expressions for the IR-HARQ protocol in a Rayleigh fading channel under a noise-limited setting. In contrast, the present work considers an interference-limited Rayleigh–Rayleigh environment, where both the desired signal and the dominant interferer experience Rayleigh fading. Moreover, while ref. [18] focused exclusively on the IR-HARQ retransmission protocol, this paper investigates the ARQ-I and CC-HARQ protocols. The outage probability formulation used here also differs from that in [18], relying on analytical results derived for interference-limited fading channels. These differences lead to distinct power allocation expressions and system behaviour, thereby extending the analysis of retransmission-based URC to a broader interference-limited scenario.

The Rayleigh–Rayleigh fading model represents a fundamental non-line-of-sight (NLOS) propagation scenario in which both the desired and interfering signals experience rich scattering without a dominant line-of-sight component. This model is practically relevant in dense urban, indoor, and obstructed wireless environments. From an analytical perspective, Rayleigh fading leads to statistically tractable channel gain distributions, enabling derivation of outage probability expressions and closed-form optimization results. For this reason, the Rayleigh–Rayleigh model serves as an analytically tractable reference framework, a worst-case baseline, for developing and validating optimal power allocation strategies, and provides a foundation for extension to more general fading environments that include line-of-sight components.

Nonetheless, environments where both the desired and interfering signals experience Rayleigh fading represent a significant type of interference-limited system [31,32]. This is because Rayleigh fading is a common phenomenon in communication networks in dense urban areas, where multipath propagation causes rapid fluctuations in signal strength due to scattering. Now, when co-channel interferer signals are present in such areas, in most cases, they too undergo Rayleigh fading [32]. Although these situations are prevalent, as previously seen in Section 1.2, such environments where both the desired and interfering signals are subjected to Rayleigh fading are often overlooked in the existing research on URC.

Thus, in this paper, we address this gap by focusing on achieving power-efficient URC in communication systems where both the desired signal and interfering signal are subject to Rayleigh fading. Throughout this paper, we call this a Rayleigh–Rayleigh system. Here, we restrict ourselves to the single-interferer case, and will address the multi-interferer case in a future work. While equations for multiple interferers exist in the literature, they are often extremely complex, making optimization and closed-form analysis intractable. For this reason, we focus on the scenario with a single dominant interferer, which simplifies the analysis while still capturing the primary interference effects. Indeed, even in the presence of many interferers, as shown in prior studies [33,34], a single interferer typically dominates the interference experienced by the receiver. In practice, this approximation is particularly valid in networks with power control, sectorization, or strong path loss, and it has been widely adopted in the literature to allow tractable analysis.

Further, we assume this communication system to be interference-limited, and that it can communicate using both ARQ-I and CC-HARQ protocols. We take the derived outage expressions for this communication system for both protocols from the literature, and modify them as functions of the retransmit power. Then, we develop an optimization problem for each protocol to find the minimum power required to achieve URC. We solve the optimization problem using the Karush–Kuhn–Tucker (KKT) method to obtain a set of equations which can be solved to obtain the minimum retransmit powers needed for a given protocol to achieve URC for a communication system located in a Rayleigh–Rayleigh fading environment. Simulations confirm that this approach yields substantial power savings for both protocols.

In the latter part of this paper, we consider the special case of two retransmissions for both protocols and formulate the optimization problem following the same procedure as above. We solve the problems with the KKT method and derive closed-form expressions for the two retransmit powers of each case. We also derive closed-form expressions for the normalized power savings with respect to the open-loop power values.

It should also be noted that although Rayleigh fading can be viewed as a special case of Rician fading when the line-of-sight component approaches zero, the corresponding optimal power allocation solutions in interference-limited Rician fading environments are typically obtained through numerical optimization and do not yield closed-form analytical expressions, as has been shown in the literature. Consequently, the closed-form solutions derived in this work for the Rayleigh–Rayleigh interference-limited case cannot be obtained by directly specializing or manipulating existing numerical solutions for more general fading models. Instead, the Rayleigh–Rayleigh model enables an independent analytical treatment that provides closed-form insights and computationally efficient benchmarks for optimal power allocation under interference-limited conditions.

1.4. Contributions

Our contributions in this paper can be summarized as follows:

- We establish a mathematical relationship between the outage probability and the retransmit power by extending the well-known outage-received power relationship in the literature, under quasi-static Rayleigh fading conditions.
- We formulate the power allocation task as an optimization problem that minimizes the average retransmit power of a transmitter operating under ARQ-I or CC-HARQ protocols, subject to a predefined target outage probability in the ultra-reliable region.

- We show that the formulated optimization problems for both protocols are non-convex, implying that the derived retransmit power solutions correspond to local minima rather than global optima.
- We derive the optimal retransmit power equations for both protocols using the KKT method, which can be numerically solved to obtain the retransmit power levels corresponding to the desired reliability target.
- We further derive closed-form analytical expressions for the retransmit powers and the corresponding normalized power savings for the special case of two maximum transmissions, providing a computationally efficient reference for real-time ultra-reliable communication applications.
- We demonstrate through numerical analysis and simulations that the proposed power allocation schemes achieve significant normalized power savings compared to conventional open-loop transmission systems, while serving as a Rayleigh–Rayleigh baseline for benchmarking against more general fading environments.

1.5. Paper Outline

The rest of this paper is organized as follows. Section 2 introduces the system model, which serves as the basis for formulating and solving the optimization problem. Section 3 provides the mathematical formulation of the optimization problem for both the ARQ-I and CC-HARQ protocols. In Section 4, the solution to the optimization problem is obtained using the KKT method, resulting in equations that can be numerically solved to determine the retransmit power values. Section 5 provides the derivation of closed-form expressions for the retransmit powers and the power savings, for the special case of two retransmissions. Section 6 gives the simulation results that verify the proposed power allocation schemes, while showing that significant power savings compared to the open-loop transmission can be achieved by employing the proposed schemes. Finally, some concluding remarks and future extensions are given in Section 7.

2. System Model

We consider a single transmitter–receiver pair inside a cell of a mobile cellular network, which is able to communicate with the Type-I ARQ protocol or CC-HARQ protocol.

The principle of Type-I ARQ is that the transmitter T_X sends the entire packet in each retransmission round, stopping either when the maximum number of retransmission rounds M is reached or when it receives confirmation that the packet has been successfully decoded [11]. The receiver R_X makes its decision based on the last received packet and discards any previously received packets. If the retransmission mechanism fails to correct the error by the end of the M-th retransmission round, the packet is discarded, and an error is declared.

The CC-HARQ protocol operates by transmitting a scaled version of the initial codeword in each retransmission round. The R_X buffers the received packets and applies maximal ratio combining to enhance the SNR [14]. In this process, the T_X sends a packet and waits for an acknowledgment from the R_X before proceeding with the next transmission. If the packet is not successfully decoded, the R_X buffers it and sends a negative acknowledgment to the T_X, requesting a retransmission. The T_X continues retransmitting until either M is reached or successful decoding is confirmed. At the R_X, the buffered packets are combined with the newly received packet to recover the original information.

Notably, in traditional ARQ protocols, R_X makes decoding decisions based solely on the most recent packet and discards previously received ones [20]. If the retransmission mechanism fails to correct the error by the M-th round, the packet is dropped, and an error is declared. We use this information when we formulate the problem in Section 3. Also, in practice, M is typically set to less than 5 to minimize delays [12], which is considered in our simulations.

As shown in Figure 1, when a signal is transmitted from the T_X to the R_X, we assume that the desired signal undergoes Rayleigh fading and is interfered with by a co-channel interferer signal, which also undergoes Rayleigh fading. Throughout this paper, we refer to such a scenario as a Rayleigh–Rayleigh system. As mentioned earlier, this work specifically targets the derivation of closed-form analytical expressions for optimal power allocation, which provides a tractable analytical baseline for the NLOS case where both desired and interfering links are Rayleigh faded. This setting serves as a worst-case benchmark against which more general fading models can later be compared.

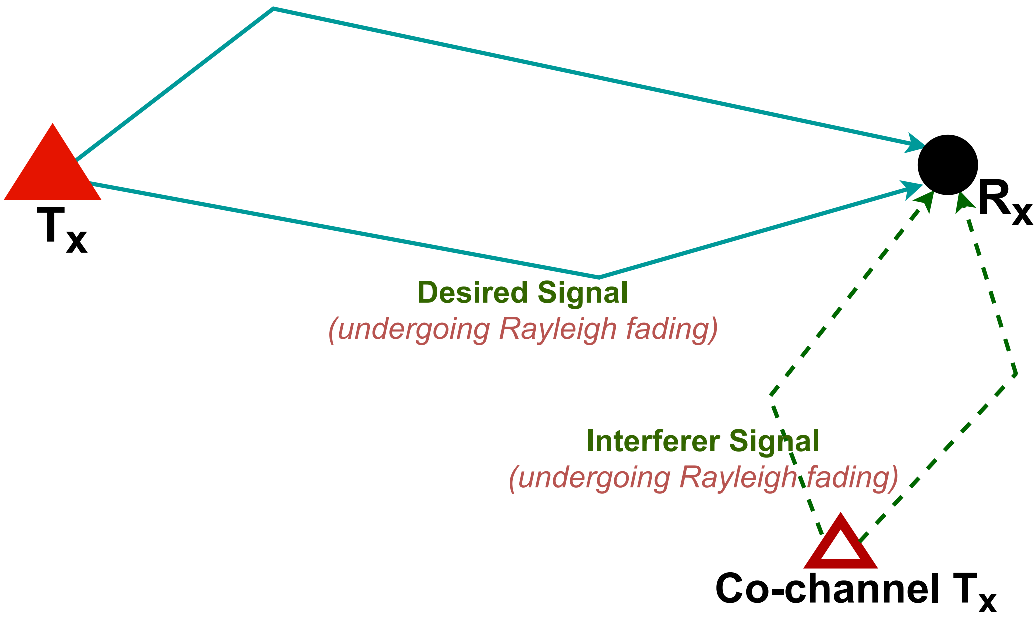

Figure 1. Considered Rayleigh–Rayleigh interference-limited communication Scenario. Solid arrows represent the desired signal path, while dashed arrows represent the interfering signal path.

Consider a mobile cellular network with a T_X–R_X pair, where the desired signal undergoes Rayleigh fading with a co-channel interferer signal undergoing Rayleigh fading. The desired signal is indicated by solid arrows and the interferer signal is indicated by dashed arrows.

Further, we assume that the system is interference-limited, making the effect of additive white Gaussian noise negligible. To maintain analytical tractability and enable the derivation of closed-form power allocations, we model interference as a single Rayleigh faded interferer. This assumption is well established in interference-limited analyses, since in practice, the outage probability is often dominated by the strongest interferer, for instance, the nearest concurrently transmitting user or a spatially proximate cell. Moreover, under realistic propagation with high path-loss exponents or directional antennas, the aggregate interference effectively reduces to the contribution of a single dominant source. Thus, the single-interferer model not only yields insightful closed-form solutions for power optimization but also provides a conservative benchmark for interference-limited scenarios in URC systems.

Furthermore, we consider that the system employs orthogonal frequency division multiple access, meaning all users share the same bandwidth.

3. Problem Formulation

Let the number of antennas in the T_X be n_t, the powers associated with the transmitter antennas be $P_{t1}, P_{t2}, \ldots, P_{tn_t}$ and the channel gains associated with them be $g_1, g_2, \ldots, g_{n_t}$. Then, the relationship between the retransmit powers and the received power P_R can be expressed as

$$\begin{bmatrix} g_1 & g_2 & \ldots & g_{n_t} \end{bmatrix} \begin{bmatrix} P_{t1} \\ P_{t2} \\ \vdots \\ P_{tn_t} \end{bmatrix} = P_R. \quad (1)$$

Our work focuses on achieving power-efficient URC by minimizing retransmit power in a Rayleigh–Rayleigh fading environment for T_X transmitting packets using the ARQ-I or CC-HARQ protocols. However, in this study, we specifically focus on minimizing the total retransmit power P_T of the transmission antenna, expressed as the sum $P_{t1} + P_{t2} + \ldots + P_{tn_t}$ in the transmission vector of Equation (1). As a result, the gain vector in the same equation reduces to a single element.

3.1. Outage Probability Expression

To find a means to minimize the total retransmit power P_T of the T_X, it is essential to establish a relationship between the transmit power and the outage probability. An expression for the outage probability of a cellular mobile radio system, where both the desired signal within a given cell and the interfering signal from a co-channel experience Rayleigh fading, can be derived from the existing literature. For this derivation, we utilize an outage probability expression for a Rayleigh faded desired signal with a Rician faded interferer that was introduced in [35]. This same expression was later derived in [36] by applying several assumptions to a more general result. This outage probability expression $P_{out-Ray/Ri}$ is given by

$$\mathcal{P}_{out-Ray/Ri} = 1 - \frac{b}{R+b} \exp\left(-\frac{cR}{R+b}\right), \quad (2)$$

where,

$$c = I/s, \quad (3)$$

and

$$b = \sigma/s. \quad (4)$$

In these expressions, R denotes the SIPR of the system, I denotes the dominant component of the interferer signal power, s denotes the scattered component of the interferer signal power, and σ denotes the scattered component of the desired signal power. These signal powers according to the derivations are at the R_X. Since we consider the interferer signal to be Rayleigh faded, we set $I = 0$. This makes $c = 0$, which makes the exponential part disappear from the equation. Thus, we obtain P_{out}, the outage probability expression for a Rayleigh–Rayleigh environment as,

$$\mathcal{P}_{out} = \frac{R}{R+b}. \quad (5)$$

However, since our goal is to achieve ultra-reliability by minimizing the total retransmit power of the transmitter P_T, we should convert the expression of the outage probability in (5), which is represented as a function of the received power, to a function of the retransmit power.

We adopt a quasi-static fading model, which assumes the channel remains constant over each short-packet transmission. This assumption is widely used in URLLC studies [11,37], as the coherence time of the channel is typically larger than the duration of a single packet. Quasi-static fading allows tractable derivation of the transmit–receive power relationship while accurately approximating the dominant channel effects for URLLC transmissions. We take the channel gain to be g, and due to the quasi-static fading model, $\sigma = gP_T$. This makes

$$b = \frac{gP_T}{s}, \tag{6}$$

and, hence, the expression for P_{out} in (5) can be modified to

$$\mathcal{P}_{out} = \frac{w}{w + P_T} \tag{7}$$

where,

$$w = \frac{Rs}{g}. \tag{8}$$

3.2. Adaptive Power Allocation Scheme

3.2.1. Average Total Retransmit Power P_{avg}

The T_X under consideration employs ARQ-I and CC-HARQ protocols, which involve multiple retransmission rounds, to successfully deliver a single packet. Consequently, when constructing the optimization problem, we formulate it as the minimization of the average total retransmit power P_{avg}. A conventional approach to power allocation is to distribute equal power across each retransmission round, resulting in an average total retransmit power of P_{budget}/M for the m-th retransmission round, where P_{budget} represents the total power budget and M denotes the maximum number of retransmission rounds and $1 \leq m \leq M$. Although this method is straightforward, works such as [19,24] have demonstrated that this uniform power allocation is highly inefficient when the outage probability is very low. Due to this, we can consider this method to be inefficient for URC, which naturally uses very low outage probabilities. To address this inefficiency and achieve power savings, we propose an adaptive power allocation scheme that assigns different power levels to each retransmission round based on system conditions, as follows.

Consider a T_X designed to communicate using ARQ-I or CC-HARQ protocols. Let the maximum number of ARQ rounds employed by the T_X be M. Here, M is defined as the total number of transmission attempts, including the initial transmission, so that $M - 1$ corresponds to the number of retransmissions. The retransmit power of the m-th ARQ round is $(P_T)_m$ where $1 \leq m \leq M$. Then, the average total retransmit power P_{avg} of a T_X which utilizes an ARQ protocol would be

$$P_{avg} = \sum_{m=1}^{M} (P_T)_m \mathcal{P}_{out,m-1}, \tag{9}$$

where $\mathcal{P}_{out,m}$ is the probability of the R_X being unable to decode a packet after m ARQ rounds. This expression was used without proof in [11,20], and in this work, we provide a proof for this expression in Appendix A.

The average retransmit power, which is given by Equation (9), reflects the expected power consumption over all possible transmission attempts, accounting for the probabilistic nature of retransmissions. Specifically, each retransmission occurs only if the previous transmission fails, and, therefore, contributes to the average power in proportion to its probability of occurrence. As a result, the average power is expressed as the sum of the transmit powers at each transmission attempt weighted by the probability that the corresponding transmission occurs. This formulation captures the expected power expenditure required to achieve the target reliability under the ARQ-I protocol.

Further, since HARQ schemes are fundamentally built upon ARQ schemes by incorporating additional mechanisms to enhance reliability and efficiency, they retain the core principles of ARQ. As a result, the above expression remains valid even for transmitters operating with HARQ protocols, and, hence, it is used in works such as [12–14]. Thus, we will also use the same expression in (9) for the P_{avg} of a T_X working on the CC-HARQ protocol.

3.2.2. Probability of Losing a Packet After m ARQ-I Rounds

In order to apply the expression in (9), it is essential to know $\mathcal{P}_{out,m}$, which is the probability of the R_X being unable to decode a packet after m ARQ rounds. According to the principle of the ARQ-I protocol, $\mathcal{P}_{out,m}$ is given by

$$\mathcal{P}_{out,m} = \prod_{k=1}^{m} (\mathcal{P}_{out})_k, \tag{10}$$

where $(\mathcal{P}_{out})_m$ is the outage probability associated with the m-th ARQ round, which, with the aid of (7), is given by

$$(\mathcal{P}_{out})_m = \frac{w}{w + (P_T)_m}. \tag{11}$$

Then, from Expression (9), the average total retransmit power P_{avg} can be written as

$$P_{avg} = \sum_{m=1}^{M} P_m \prod_{k=1}^{m-1} \frac{w}{w + P_k}, \tag{12}$$

where $(P_T)_m$ is denoted as P_m for simplicity of notation, and the probability of the R_X being unable to decode a packet before the packet is transmitted is unity, $P_{out,0} = 1$.

3.2.3. Probability of Losing a Packet After m CC-HARQ Rounds

The application of (9) to find P_{avg} is challenging in this case, as we need to find a suitable $\mathcal{P}_{out,m}$ which reflects the key features of CC-HARQ.

A corresponding $\mathcal{P}_{out,m}$ can be found in Equation (07) of [24]; however, this expression is highly complex to work with. Due to this, its authors derived an approximation for this expression in Appendix B of [24] using the standard Gauss–Legendre approximation, employing a Legendre polynomial of a specific order and selecting an appropriate value for that order. This derived expression is

$$\mathcal{P}_{out,m} = \frac{1}{m!} \prod_{k=1}^{m} (\mathcal{P}_{out})_k, \tag{13}$$

with an approximation error smaller than 10^{-6}. Due to this accepted level of accuracy, we adopt this expression for calculating P_{avg} for CC-HARQ. Now, with this and (11), the expression for P_{avg} in (9) for CC-HARQ turns out to be

$$P_{avg} = \sum_{m=1}^{M} P_m \frac{1}{(m-1)!} \prod_{k=1}^{m-1} \frac{w}{w + P_k}. \tag{14}$$

Here too, $(P_T)_m$ is denoted as P_m for simplicity of notation and the probability of the R_X being unable to decode a packet before the packet is transmitted is unity, $P_{out,0} = 1$.

3.3. Optimization Problems

The aim of this work is to minimize the average total retransmit power P_{avg} of the T_X. To achieve this aim, we formulate it as an optimization problem for each protocol, considering each as a minimization of the P_{avg} corresponding to each protocol. The constraints for the problem are the non-negativity of the retransmit powers and the packet drop probability $\mathcal{P}_{out,M}$ being equal to a pre-defined target outage probability ξ. The packet drop probability represents the probability of the R_X being unable to decode a packet despite exhausting all M transmission attempts [11]. Even though the second constraint could also be rigorously written as an inequality $\mathcal{P}_{out,M} \leq \xi$, it is well-established in power minimization problems, given in works such as [11,12], that the optimal solution occurs at the boundary of the feasible set. This boundary is reached when the constraint is tightly binding, i.e., as an equality. $\mathcal{P}_{out,M} < \xi$ would imply being more reliable than required, which spends more power than necessary, which the minimization naturally avoids. Further, in the simulations in Section 6, we set the values for ξ within the URC region and present the results.

With these considerations, the optimization problem for ARQ-I can be formulated as

$$\begin{aligned} &\underset{P_m}{\text{Minimize}} \quad \sum_{m=1}^{M} P_m \prod_{k=1}^{m-1} \frac{w}{w+P_k} \\ &\text{Subject to} \qquad P_m \geqslant 0 \quad ;1 \leq m \leq M \\ &\qquad\qquad \prod_{m=1}^{M} \frac{w}{w+P_m} = \xi. \end{aligned} \tag{15}$$

Similarly, the optimization problem for CC-HARQ is

$$\begin{aligned} &\underset{P_m}{\text{Minimize}} \quad \sum_{m=1}^{M} P_m \frac{1}{(m-1)!} \prod_{k=1}^{m-1} \frac{w}{w+P_k} \\ &\text{Subject to} \qquad P_m \geqslant 0 \quad ;1 \leq m \leq M \\ &\qquad\qquad \frac{1}{M!} \prod_{m=1}^{M} \frac{w}{w+P_m} = \xi. \end{aligned} \tag{16}$$

For both cases, the optimization variables are P_m for $m = 1, 2, \ldots, M$.

3.4. Non-Convexity of the Problems

Before solving the problem, we first determine whether the optimization problem is convex. To do this, we use the Hessian matrix method [38]. We show the non-convexity proof explicitly for the special case of $M = 2$ for both the protocols. However, the underlying structure of the average power objective function and outage probability constraints remains fundamentally similar for larger numbers of retransmissions, i.e., for a general M. In particular, the objective function involves products and nested non-linear functions of the retransmit powers, which lead to indefinite Hessian matrices and non-convex behavior. Extending the proof to the general M-retransmissions follows the same procedure but results in increasingly complex expressions due to the higher-dimensional Hessian matrix.

Therefore, the $M = 2$ case, which we prove in Appendix B, serves as a representative demonstration of the inherent non-convexity of the optimization problem, and the same non-convex characteristics extend to the general case. The results confirm that the optimization problem is non-convex for ARQ-I and CC-HARQ [39]. Additionally, we observe that the equality constraints in (15) and (16) are non-affine. Given these conditions, we propose a method to obtain a local optimum solution [38,39].

4. Sub-Optimal Solution via KKT Method

4.1. For ARQ-I

Here, we make use of the Karush–Kuhn–Tucker (KKT) conditions to obtain a local minimum for the optimization problem presented in (15). For this purpose, first, we write its Lagrangian function as

$$\mathcal{L}(P_m, \mu_m, \lambda) = \sum_{m=1}^{M} P_m \prod_{k=1}^{m-1} \frac{w}{w + P_k} + \sum_{m=1}^{M} \mu_m P_m + \lambda \left(\prod_{m=1}^{M} \frac{w}{w + P_m} - \xi \right). \tag{17}$$

The KKT conditions for the optimization problem in (15) can be expressed as

$$C_1 \rightarrow \quad \nabla \mathcal{L} = 0 \tag{18}$$

$$C_2 \rightarrow \quad P_m \geqslant 0 \tag{19}$$

$$C_3 \rightarrow \quad \prod_{m=1}^{M} \frac{w}{w + P_m} - \xi = 0 \tag{20}$$

$$C_4 \rightarrow \quad \mu_m \geqslant 0 \tag{21}$$

$$C_5 \rightarrow \quad \mu_m P_m = 0. \tag{22}$$

Since in each ARQ round, some amount of power should be present to transmit the signals, $P_m > 0$ for $m = 1, 2, \ldots, M$. Therefore, from (22), we get $\mu_m = 0$ for $m = 1, 2, \ldots, M$. Hence, the Lagrangian function in (17) simplifies to

$$\mathcal{L}(P_m, \lambda) = \sum_{m=1}^{M} P_m \prod_{k=1}^{m-1} \frac{w}{w + P_k} + \lambda \left(\prod_{m=1}^{M} \frac{w}{w + P_m} - \xi \right). \tag{23}$$

Applying the stationary condition in (18) with respect to P_m for (23) and simplifying, we can deduce that

$$\left[\prod_{j=1}^{m-1} \frac{w}{w + P_j} - \frac{1}{w + P_m} \sum_{j=1}^{M-m} P_{j+m} \prod_{l=1}^{j+m-1} \frac{w}{w + P_l} \right] - \lambda \frac{1}{w + P_m} \prod_{j=1}^{M} \frac{w}{w + P_j} = 0. \tag{24}$$

Now, this is for $1 \leq m \leq M$. Therefore, by substituting $m = M, M-1, M-2, \ldots, 3, 2, 1$, we get

$$(w + P_M)^2 = \lambda w, \tag{25}$$

$$(w + P_{M-1})^2 = w P_M + \frac{\lambda w^2}{(w + P_M)}, \tag{26}$$

$$(w + P_{M-2})^2 = w P_{M-1} + \frac{w^2 P_M}{(w + P_{M-1})} + \frac{\lambda w^3}{(w + P_M)(w + P_{M-1})}, \tag{27}$$

and likewise. Now, we can simplify in the following manner using $w + P_m > 0$.

$$\begin{aligned}
(w + P_{M-1})^2 &= w P_M + \frac{\lambda w^2}{(w + P_M)} \\
&= w P_M + \lambda w \frac{w}{(w + P_M)} \\
&= w P_M + (w + P_M)^2 \frac{w}{(w + P_M)} \\
&= w P_M + w(w + P_M) \\
&= w(w + 2P_M).
\end{aligned} \tag{28}$$

Repeating this, we obtain

$$w + P_M = \sqrt{\lambda w}, \tag{29}$$

$$w + P_{M-1} = \sqrt{w(w + 2P_M)}, \tag{30}$$

$$w + P_{M-2} = \sqrt{w(w + 2P_{M-1})}, \tag{31}$$

and likewise. These relations can be identified to have the general relation $w + P_m = \sqrt{w(w + 2P_{m+1})}$. Again, we do a similar substitution as above.

$$\begin{aligned} w + P_{M-1} &= \sqrt{w(w + 2P_M)} \\ &= \sqrt{w(w + 2(\sqrt{\lambda w} - w))} \\ &= \sqrt{w(2\sqrt{\lambda w} - w))} \\ w + P_{M-1} &= \sqrt{2w\sqrt{\lambda w} - w^2} \\ P_{M-1} &= \sqrt{2w\sqrt{\lambda w} - w^2} - w. \end{aligned} \tag{32}$$

By repeating this, we obtain

$$P_M = \sqrt{\lambda w} - w, \tag{33}$$

$$P_{M-1} = \sqrt{2w\sqrt{\lambda w} - w^2} - w, \tag{34}$$

$$P_{M-2} = \sqrt{2w\sqrt{2w\sqrt{\lambda w} - w^2} - w^2} - w, \tag{35}$$

and so on. Therefore, by considering the pattern, P_m can be obtained as

$$\begin{aligned} &P_m \\ &= P_{M-(M-m)} \\ &= \sqrt{2w \ldots \sqrt{2w\sqrt{2w\sqrt{\lambda w} - w^2} - w^2} \ldots - w^2} - w. \end{aligned} \tag{36}$$

Note that there are $M - m$ number of square roots nested to $\sqrt{\lambda w}$. Since we can write (20) as

$$\prod_{m=1}^{M} (w + P_m) = \frac{w^M}{\xi}. \tag{37}$$

from (36) and (37), we get

$$\prod_{m=1}^{M} \sqrt{2w \ldots \sqrt{2w\sqrt{2w\sqrt{\lambda w} - w^2} - w^2} \ldots - w^2} = \frac{w^M}{\xi}, \tag{38}$$

from which we can find λ numerically, and by substituting this answer into (36), we can find $P_m \quad \forall m = 1, 2, \ldots, M$.

4.2. For CC-HARQ

Here too, we make use of the KKT conditions as above, and we focus on the optimization problem presented in (16). Also note that the simplifications are similar to those of ARQ-I. The Lagrangian function for this scenario is

$$\mathcal{L}(P_m,\mu_m,\lambda') = \sum_{m=1}^{M} P_m \frac{1}{(m-1)!}\prod_{k=1}^{m-1}\frac{w}{w+P_k} + \sum_{m=1}^{M}\mu_m P_m + \lambda'\left(\frac{1}{M!}\prod_{m=1}^{M}\frac{w}{w+P_m} - \xi\right), \tag{39}$$

and the KKT conditions are

$$C_1 \rightarrow \qquad \nabla\mathcal{L} = 0 \tag{40}$$

$$C_2 \rightarrow \qquad P_m \geqslant 0 \tag{41}$$

$$C_3 \rightarrow \qquad \frac{1}{M!}\prod_{m=1}^{M}\frac{w}{w+P_m} - \xi = 0 \tag{42}$$

$$C_4 \rightarrow \qquad \mu_m \geqslant 0 \tag{43}$$

$$C_5 \rightarrow \qquad \mu_m P_m = 0. \tag{44}$$

Applying the same logic as in Section 4.1, we simplify the Lagrangian function in (39) to

$$\mathcal{L}(P_m,\lambda') = \sum_{m=1}^{M} P_m \frac{1}{(m-1)!}\prod_{k=1}^{m-1}\frac{w}{w+P_k} + \left(\frac{\lambda'}{M!}\prod_{m=1}^{M}\frac{w}{w+P_m} - \xi\right). \tag{45}$$

Applying the stationary condition in (40) with respect to P_m for (45) and simplifying gives

$$\begin{aligned}\frac{1}{(m-1)!}\prod_{j=1}^{m-1}\frac{w}{w+P_j} - \frac{1}{w+P_m}\Bigg[\sum_{j=1}^{M-m} P_{j+m}\frac{1}{(j+m-1)!}\\ \prod_{l=1}^{j+m-1}\frac{w}{w+P_l}\Bigg] - \frac{\lambda'}{M!}\frac{1}{w+P_m}\prod_{j=1}^{M}\frac{w}{w+P_j} = 0.\end{aligned} \tag{46}$$

By substituting $m = M, M-1, M-2, \ldots, 3, 2, 1$, we get

$$(w+P_M)^2 = \frac{\lambda' w}{M}, \tag{47}$$

$$(w+P_{M-1})^2 = \frac{wP_M}{M-1} + \frac{\lambda' w^2}{M(M-1)(w+P_M)}, \tag{48}$$

$$(w+P_{M-2})^2 = \frac{wP_{M-1}}{M-2} + \frac{w^2 P_M}{(w+P_{M-1})} + \frac{\lambda' w^3}{(M-1)(M-2)(w+P_M)(w+P_{M-1})}, \tag{49}$$

and likewise. Substituting each result from the previous step into the next step considering $w+P_m > 0$ gives

$$w+P_M = \sqrt{\frac{\lambda' w}{M}}, \tag{50}$$

$$w+P_{M-1} = \sqrt{\frac{w}{M-1}(w+2P_M)}, \tag{51}$$

$$w+P_{M-2} = \sqrt{\frac{w}{M-2}(w+2P_{M-1})}, \tag{52}$$

and likewise. These relations can be recognized as following the general form $w+P_m = \sqrt{\frac{w}{m}(w+2P_{m+1})}$. By further substituting the results from the previous steps, we obtain

$$P_M = \sqrt{\frac{\lambda' w}{M}} - w, \tag{53}$$

$$P_{M-1} = \sqrt{\frac{w}{M-1}\left(2\sqrt{\frac{\lambda' w}{M}} - w\right)} - w, \tag{54}$$

$$P_{M-2} = \sqrt{\frac{w}{M-2}\left(2\sqrt{\frac{w}{M-1}\left(2\sqrt{\frac{\lambda' w}{M}} - w\right)} - w\right)} - w, \tag{55}$$

and so on. Thus, by observing the pattern, we can express P_m as

$$\begin{aligned} &P_m \\ &= P_{M-(M-m)} \\ &= \sqrt{\frac{w}{m}\cdots\left(2\sqrt{\frac{w}{M-1}\left(2\sqrt{\frac{\lambda' w}{M}} - w\right)} - w\right)\cdots - w} - w. \end{aligned} \tag{56}$$

Here too, there are $M-m$ number of square roots nested to $\sqrt{\lambda' w}$. Thus, using (42), we obtain

$$\prod_{m=1}^{M}(w + P_m) = \frac{w^M}{\xi\ M!}. \tag{57}$$

Therefore, from (56) and (57), we get

$$\prod_{m=1}^{M}\sqrt{\frac{w}{m}\cdots\left(2\sqrt{\frac{w}{M-1}\left(2\sqrt{\frac{\lambda' w}{M}} - w\right)} - w\right)\cdots - w} = \frac{w^M}{\xi\ M!}. \tag{58}$$

From this, we can determine λ' numerically. Substituting this value into (56), we obtain $P_m \quad \forall m = 1, 2, \ldots, M$.

5. The Special Case of M = 2

As discussed earlier, obtaining closed-form solutions for general M retransmissions is not feasible. Therefore, we focus on the specific case of $M = 2$ and derive closed-form solutions for this scenario. While λ for ARQ-I can be determined using (38) and P_1 and P_2 can be found using (36), with a similar approach applicable to CC-HARQ using (58) and (56), we instead follow the steps in the general problem formulation. This approach provides a structured method for obtaining a closed-form expression for the particular case of $M = 2$. We begin with ARQ-I and then proceed to CC-HARQ.

5.1. For ARQ-I

5.1.1. Problem Formulation

We start by writing the simplified objective function for $M = 2$ as

$$\mathcal{L} = P_1 + P_2\left(\frac{w}{w+P_1}\right) + \lambda\left(\frac{w}{w+P_1}\cdot\frac{w}{w+P_2} - \xi\right), \tag{59}$$

and obtaining the stationary conditions $\frac{\partial \mathcal{L}}{\partial P_1} = \frac{\partial \mathcal{L}}{\partial P_2} = 0$. Then, we obtain λ from $\frac{\partial \mathcal{L}}{\partial P_2} = 0$ as $\lambda = \frac{(w+P_2)^2}{w}$. Plugging this value into the λ in $\frac{\partial \mathcal{L}}{\partial P_1} = 0$ and simplifying, we obtain

$$P_2 = \frac{2wP_1 + {P_1}^2}{2w}. \tag{60}$$

Substituting this value of P_2 into (20), we get

$$P_1^3 + 3wP_1^2 + 4w^2P_1 - 2w^3\left(\frac{1-\xi}{\xi}\right) = 0. \tag{61}$$

5.1.2. Solving Using the General Cubic Solutions

Since this is a cubic equation, we utilize the general cubic formula for solving cubic equations to obtain the solution for Equation (61). According to [40], the general solution to the cubic equation $a_3x^3 + a_2x^2 + a_1x + a_0 = 0$ is given by

$$x_k = -\frac{1}{3a_3}\left(a_2 + \zeta^k C + \frac{\Delta_0}{\zeta^k C}\right);\ k \in \{0, 1, 2\} \tag{62a}$$

$$\zeta = \frac{-1+\sqrt{3}i}{2};\quad \zeta^2 = \frac{-1-\sqrt{3}i}{2} \tag{62b}$$

$$C = \sqrt[3]{\frac{\Delta_1 \pm \sqrt{{\Delta_1}^2 - 4{\Delta_0}^3}}{2}} \tag{62c}$$

$$\Delta_0 = {a_2}^2 - 3a_3a_1 \tag{62d}$$

$$\Delta_1 = {a_2}^3 - 9a_3a_2a_1 + 27{a_3}^2a_0 \tag{62e}$$

We start by solving for P_1; therefore, by comparing (61) with the general cubic equation, we find the coefficients to be $a_3 = 1, a_2 = 3w, a_1 = 4w^2$ and $a_0 = -2w^3\left(\frac{1-\xi}{\xi}\right)$. Subsequently, it follows from the above equations that $\Delta_0 = -3w^2$ and $\Delta_1 = -27w^3\left(\frac{2+\xi}{\xi}\right)$. Thus, we calculate C to be

$$C = -\frac{3w}{\sqrt[3]{2}}\left[\left(\frac{2+\xi}{\xi}\right) \mp \sqrt{\left(\frac{2+\xi}{\xi}\right)^2 + \frac{4}{27}}\right]^{\frac{1}{3}}. \tag{63}$$

5.1.3. Selecting an Appropriate C

As per the rules for the selection of C, the selection could be done arbitrarily between the positive square root and the negative square root, given that the result is not indeterminate. Thus, we see that we can freely choose either square root. To proceed further, we select the positive square root and express C as

$$C = -3w\chi \tag{64}$$

where,

$$\chi = \left[\left(\frac{2+\xi}{2\xi}\right) + \frac{1}{2}\sqrt{\left(\frac{2+\xi}{\xi}\right)^2 + \frac{4}{27}}\right]^{\frac{1}{3}}. \tag{65}$$

5.1.4. Solutions to P_1 and P_2

According to (62a), there are three solutions to (61) as $(P_1)_0$, $(P_1)_1$ and $(P_1)_2$. Therefore, by substituting $k = 0$ and simplifying, we get $(P_1)_0 = wA$, where

$$A = \chi - 1 - \frac{1}{3\chi}. \tag{66}$$

Now, when considering $k = 1, 2$, we get $(P_1)_1$ and $(P_1)_2$, which can be identified as complex numbers with non-zero imaginary parts when observed (62a). Since $P_1 \in \Re$, we can discard these two solutions; thus, the only candidate for P_1 would be $(P_1)_0$.

Further, since $P_1 > 0$, we need to check whether $(P_1)_0$ is positive or not. For this purpose, we assume $(P_1)_0$ to be positive; hence,

$$
\begin{aligned}
&(P_1)_0 \\
&\Rightarrow wA > 0 \\
&\Rightarrow A > 0; \qquad \because\ w = \frac{Rs}{g} > 0 \\
&\Rightarrow \chi - 1 - \frac{1}{3\chi} > 0 \\
&\Rightarrow 3\chi^2 - 3\chi - 1 > 0; \qquad \because\ \chi > 0 \\
&\Rightarrow \left(\chi - \frac{3-\sqrt{21}}{6}\right)\left(\chi - \frac{3+\sqrt{21}}{6}\right) > 0 \\
&\Rightarrow \chi < \frac{3-\sqrt{21}}{6} \bigcup \frac{3+\sqrt{21}}{6} < \chi.
\end{aligned}
\tag{67}
$$

According to this, χ should be in the above range for $(P_1)_0$ to be positive. However, we know that since $0 \leq \xi \leq 1$, the range of χ can be found by inspecting (65); accordingly the lower and upper bounds of χ are $\sqrt[3]{\frac{3}{2} + \frac{1}{2}\sqrt{9 + \frac{4}{27}}}$ and ∞, respectively. By computing the numerical values, we can show that $\frac{3+\sqrt{21}}{6} < \sqrt[3]{\frac{3}{2} + \frac{1}{2}\sqrt{9 + \frac{4}{27}}}$; hence, we see that the range of χ is in the required range. We can conclude that $(P_1)_0 > 0$, and, thus, $P_1 = (P_1)_0$, which gives

$$P_1 = wA. \tag{68}$$

Now, by substituting this value of P_1 into (60), we get

$$P_2 = \frac{wA}{2}(A + 2). \tag{69}$$

It is also evident from the above that since $w > 0$ and $A > 0$, $P_2 > 0$.

The derived Equation (61) yields three mathematical roots, two of which are complex roots and one a real root. However, since retransmit powers represent physical quantities, only real and non-negative solutions are feasible. Complex roots do not correspond to physically realizable retransmit powers, and negative roots are not meaningful in this context. Among the feasible real-valued roots, the selected solutions are the ones that satisfy the outage probability constraint and minimize the average retransmit power, thereby fulfilling the optimality conditions of the original constrained optimization problem.

We can also prove that $P_2 > P_1$. The proof is given in Appendix C.

5.1.5. Normalized Power Saving

The target outage probability is ξ; the required transmit power for an open-loop communication system can be obtained from (7) as

$$P = \frac{w}{\xi}(1 - \xi). \tag{70}$$

With respect to the open-loop setup

To quantify the efficiency improvement of the proposed retransmission schemes over conventional open-loop transmission, we define normalized power saving with respect to the open-loop setup S_m for each transmission round m. If we succeeded in the first transmission round itself, then we define the normalized power saving S_1 as

$$S_1 = \frac{P - P_1}{P} = 1 - \frac{A\xi}{1-\xi}, \tag{71}$$

and if we succeeded in the second transmission round, we define the power saving S_2 as

$$S_2 = \frac{P - (P_1 + P_2)}{P} = 1 - \frac{A(A+4)\xi}{2(1-\xi)}. \tag{72}$$

Here, P denotes the open-loop transmit power, and P_1, P_2 are the allocated transmit powers in the respective rounds. A higher S_m indicates a larger reduction in total transmit power relative to open-loop transmission and, thus, a greater power efficiency.

We observe that both S_1 and S_2 are functions of A and ξ only. Further, since A is a function of χ according to (66) and χ is a function of ξ according to (65), it turns out that S_1 and S_2 are functions of ξ only. Therefore, it follows that the power savings do not change with the signal-to-interference protection ratio R, the scattered signal power of the interferer signal s, or the channel gain g.

With respect to Equal power allocation

For benchmarking purposes, we also consider a simple equal power allocation strategy for the $M = 2$ case, where the total open-loop power is equally divided between the two attempts. Under equal power allocation, the transmit powers remain fixed and independent of retransmission statistics.

Using the same outage probability framework as developed in the previous subsection, the normalized average power saving under EPA can be derived analytically. The corresponding expressions for the expected transmit power and normalized saving can be written and simplified as

$$S_{1-equal} = \frac{P - P_1}{P} = \frac{P - \frac{P}{2}}{P} = \frac{1}{2}, \tag{73}$$

$$S_{2-equal} = \frac{P - (P_1 + P_2)}{P} = \frac{P - (\frac{P}{2} + \frac{P}{2})}{P} = 0, \tag{74}$$

where $S_{1-equal}$ and $S_{2-equal}$ are the normalized power savings at the first and second retransmissions when used equal power allocation.

Under equal power allocation, if transmission succeeds in the first attempt, only half of the total open-loop power is consumed, resulting in a 50% power saving. However, if a second transmission is required, the total consumed power equals the open-loop benchmark, yielding zero power saving. This behaviour is consistent with expectations, since equal allocation distributes power uniformly without adapting to retransmission outcomes.

5.1.6. Average Power Saving

Average power saving S_{avg} is given by

$$S_{avg} = \frac{P - (P_1 + \epsilon_1 P_2)}{P}. \tag{75}$$

Therefore, the average power savings of using equal power allocation $S_{avg-equal}$ and adaptive power allocation $S_{avg-adaptive}$, respectively are,

$$S_{avg-equal} = \frac{P - (\frac{P}{2} + \epsilon_1 \frac{P}{2})}{P} = 1 - \frac{1}{2}(1 + \epsilon_1). \quad (76)$$

$$S_{avg-adaptive} = \frac{P - \left[wA \ + \ \epsilon_1 \ \frac{wA}{2}(A+2) \right]}{P} = 1 - wA \ \frac{2 + \epsilon_1(A+2)}{2P}. \quad (77)$$

Now, if we check the value of average power saving when $\epsilon_1 \to 0$, we can see that for the equal power scheme, it goes to 0.5, and in the adaptive power scheme, it goes to 1. Thus, the maximum possible saving under equal power allocation is 50%, and for adaptive power allocation, there is a near 100% saving potential theoretically. Therefore, we can surely say that the optimal scheme saves power more compared to the equal power scheme.

5.2. For CC-HARQ

5.2.1. Problem Formulation

Similarly, as above, we start by writing the simplified objective function for $M = 2$ as

$$\mathcal{L} = P_1 + P_2\left(\frac{w}{w + P_1}\right) + \lambda'\left(\frac{1}{2}\frac{w}{w + P_1} \cdot \frac{w}{w + P_2} - \xi\right). \quad (78)$$

Then, we obtain λ' from the stationary condition $\frac{\partial \mathcal{L}}{\partial P_2} = 0$ as $\lambda' = \frac{(w+P_2)^2}{w}$, and using this value with the stationary condition $\frac{\partial \mathcal{L}}{\partial P_1} = 0$ results in

$$P_2 = \frac{w^2 + 4wP_1 + 2{P_1}^2}{2w}. \quad (79)$$

Substituting this value of P_2 into the equality constraint, we get

$$2P_1^3 + 6wP_1^2 + 7w^2P_1 - w^3\left(\frac{1 - 3\xi}{\xi}\right) = 0. \quad (80)$$

5.2.2. Solving Using the General Cubic Solutions

We obtain the solution for (80) using the general cubic formula. Here too, we find the solution for P_1, and then afterwards find the solution for P_2.

We start by solving for P_1; therefore, by comparing (80) with the general cubic equation, we find the coefficients to be $a_3 = 2, a_2 = 6w, a_1 = 7w^2$ and $a_0 = -w^3\left(\frac{1-3\xi}{\xi}\right)$. Subsequently, it follows from the above equations that $\Delta_0 = -6w^2$ and $\Delta_1 = -108w^3\left(\frac{1+2\xi}{\xi}\right)$. Thus, we calculate C to be

$$C = \frac{-6w}{\sqrt[3]{4}}\left[\left(\frac{1 + 2\xi}{\xi}\right) \mp \sqrt{\left(\frac{1 + 2\xi}{\xi}\right)^2 + \frac{2}{27}}\right]^{\frac{1}{3}}. \quad (81)$$

5.2.3. Selecting an Appropriate C

As mentioned earlier, since we can freely choose either square root, to proceed further, we select the positive square root and express C as

$$C = -6w\chi' \quad (82)$$

where

$$\chi' = \left[\left(\frac{1+2\xi}{4\xi}\right) + \frac{1}{4}\sqrt{\left(\frac{1+2\xi}{\xi}\right)^2 + \frac{2}{27}}\right]^{\frac{1}{3}}. \tag{83}$$

5.2.4. Solutions to P_1 and P_2

According to (62a), there are three solutions to (61) as $(P_1)_0$, $(P_1)_1$ and $(P_1)_2$. Therefore, by substituting $k = 0$ and simplifying, we get $(P_1)_0 = wA'$, where

$$A' = \chi' - 1 - \frac{1}{6\chi'}. \tag{84}$$

Now, when considering $k = 1, 2$, we get $(P_1)_1$ and $(P_1)_2$, which can be identified as complex numbers with non-zero imaginary parts when observed (62a). Since $P_1 \in \Re$, we can discard these two solutions; thus, the only candidate for P_1 would be $(P_1)_0$. Further, since $P_1 > 0$, we need to check whether $(P_1)_0$ is positive or not. For this purpose, we assume $(P_1)_0$ to be positive; hence,

$$\begin{aligned}
&(P_1)_0 \\
&\Rightarrow wA' > 0 \\
&\Rightarrow A' > 0; \qquad \because\ w = \frac{Rs}{g} > 0 \\
&\Rightarrow \chi' - 1 - \frac{1}{6\chi'} > 0 \\
&\Rightarrow 6\chi'^2 - 6\chi' - 1 > 0; \qquad \because\ \chi' > 0 \\
&\Rightarrow \left(\chi' - \frac{3-\sqrt{15}}{6}\right)\left(\chi' - \frac{3+\sqrt{15}}{6}\right) > 0 \\
&\Rightarrow \chi' < \frac{3-\sqrt{15}}{6} \bigcup \frac{3+\sqrt{15}}{6} < \chi'.
\end{aligned} \tag{85}$$

According to this, χ' should be in the above range for $(P_1)_0$ to be positive. However, we know that since $0 \leq \xi \leq 1$, the range of χ' can be found by inspecting (83); accordingly, the lower and upper bounds of χ' are $\sqrt[3]{\frac{3}{4} + \frac{1}{4}\sqrt{9 + \frac{2}{27}}}$ and ∞, respectively. A simple arithmetic proof can be given to show that $\sqrt[3]{\frac{3}{4} + \frac{1}{4}\sqrt{9 + \frac{2}{27}}} = \frac{3+\sqrt{15}}{6}$. The proof is given in Appendix D. We see that the range of χ' is in the required range. Therefore, we conclude that $(P_1)_0 > 0$, and, thus, $P_1 = (P_1)_0$. From this and by substituting the result for P_1 into (79), we get the following.

$$P_1 = wA'. \tag{86}$$

$$P_2 = \frac{w}{2}\left(1 + 4A' + 2A'^2\right). \tag{87}$$

It is also evident from the above that since $w > 0$ and $A > 0$, $P_2 > 0$. We can also prove that $P_2 > P_1$. The proof is given in Appendix E.

5.2.5. Normalized Power Saving

With respect to the open-loop setup

The required transmit power for an open-loop communication system is given in (70). If we succeeded in the first retransmission itself, then the normalized power saving S_1' with respect to the open-loop setup can be expressed as

$$S_1' = \frac{P - P_1}{P} = 1 - \frac{A'\xi}{1-\xi}, \tag{88}$$

and if we succeeded in the second retransmission, then

$$S_2' = \frac{P - (P_1 + P_2)}{P} = 1 - \frac{(1 + 6A' + 2A'^2)\xi}{2(1-\xi)}. \tag{89}$$

Here too, we observe that both S_1' and S_2' are functions of ξ only from the same logic in Section 5.1.5. Therefore, it follows that in CC-HARQ too, the power savings do not change with R, s or g.

With respect to equal power allocation

The expressions derived for this scenario will be the same as that derived earlier for the ARQ-I scheme which are (73) and (74).

5.2.6. Average Power Saving

This can be calculated for the equal power and adaptive power scenarios using (75) as was shown in Section 5.1.6. It can be observed that the average power saving for equal power allocation $S'_{avg-equal}$ is the same as (76). For the adaptive power allocation,

$$S'_{avg-adaptive} = \frac{P - \left[wA' + \epsilon_1 \frac{w}{2}(1 + 4A' + 2A'^2)\right]}{P}. \tag{90}$$

Here too, we see that when $\epsilon_1 \to 0$, the saving from the adaptive power scheme goes to 1. Thus, we can observe a near 100% saving potential theoretically for this protocol too. Therefore, here too, the optimal scheme saves power more compared to the 50% equal power scheme.

6. Simulations and Analysis of Results

In this section, we present simulation results to evaluate the performance of the proposed adaptive power allocation scheme in a system where both the desired and interfering signals experience Rayleigh fading. Specifically, we compare the retransmission power levels obtained by our adaptive scheme with those obtained from the conventional open-loop power transmission (OLP) approach.

To carry out this task, we begin by generating the channel gain g, which appears in (8) and is embedded in the term w that recurs in many of the derived expressions. For numerical evaluation, channel gain g values were generated using uniformly distributed random samples over the interval $[0, 1]$ to ensure unbiased sampling across the entire range of possible normalized channel conditions. These samples are used purely as numerical inputs to evaluate the derived analytical expressions and do not represent the statistical fading model itself. The underlying channel fading model assumed throughout the analysis remains Rayleigh fading, for which the channel power gain follows an exponential distribution.

Next, we numerically solve (38), which was derived as part of the power allocation scheme for ARQ-I, to determine the value of λ. This value is then substituted into (36) to obtain the retransmission power levels required to ensure ultra-reliable communication in a Rayleigh–Rayleigh fading environment. Similarly, the power allocation for the retransmission stages in the CC-HARQ scheme is obtained by solving Equations (58) and (56). The values of λ and λ' are selected such that all computed retransmission powers are non-negative, ensuring the physical feasibility of the solution. However, the closed-form formulae derived in Section 5 were used for the cases involving only two retransmissions i.e., $M = 2$. Further, the time complexity of the implemented program is constant, i.e., $\mathcal{O}(1)$, as it operates on a fixed set of input parameters [41].

Moreover, the retransmission power values obtained from this computation can be pre-calculated and stored, since the underlying calculations are not required to be performed in real time. This pre-computation approach is feasible because the optimal retransmission power depends only on slowly varying statistical channel parameters, such as fading distribution and interference characteristics. Therefore, the computed values can be stored in lookup tables and used during operation without requiring real-time numerical computation. This approach ensures low implementation complexity while maintaining accurate retransmission power estimation, provided that the channel statistics are appropriately characterized. Additionally, to ensure statistical reliability, the results averaged over 100,000 independent channel realizations.

6.1. Variation of Retransmit Power Values for M = 2, 3, 4

Figures 2 and 3 show the variation of retransmission powers P_m with respect to the target outage probability ξ for different maximum numbers of retransmissions, i.e., $M = 2, 3$ and 4, while keeping R fixed at 10. Numerical results indicate that increasing M leads to a reduction in the total power required to meet the outage constraint, i.e., $P_1 + P_2 > P_1 + P_2 + P_3 > P_1 + P_2 + P_3 + P_4$.

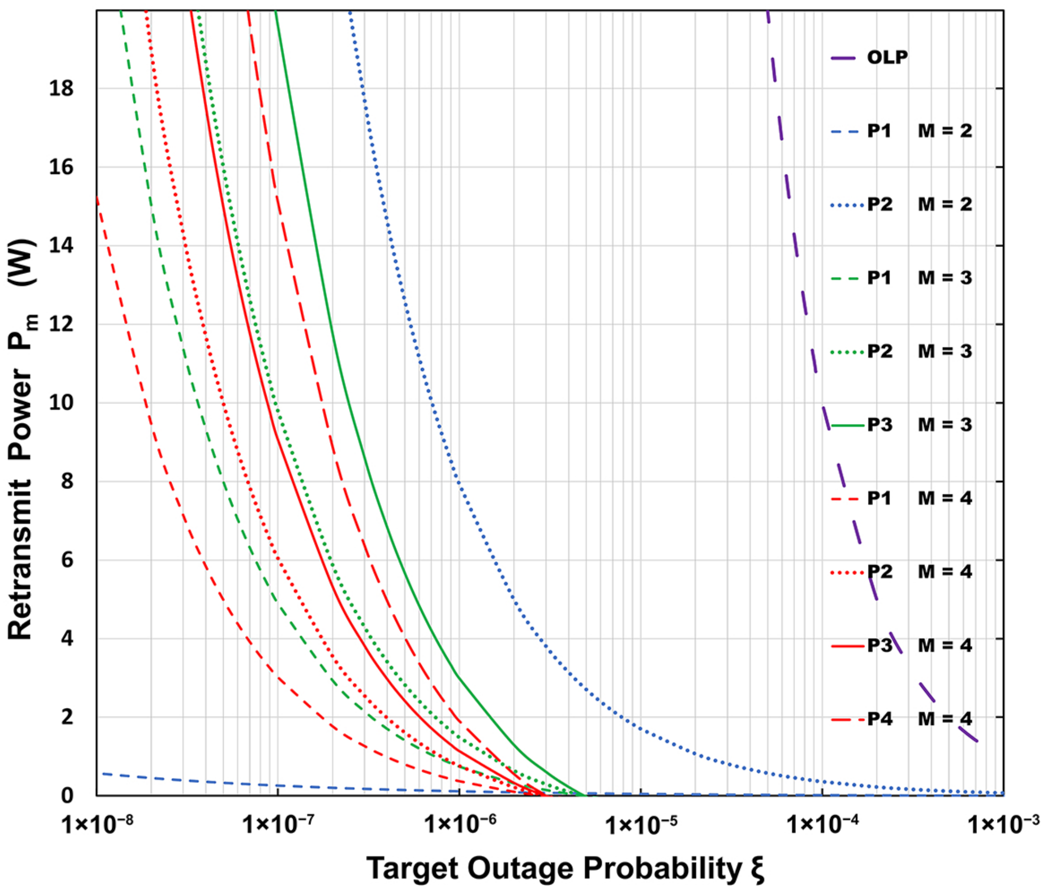

Figure 2. Retransmit power vs. target outage probability for ARQ-I when $M = 2, 3, 4$.

This figure shows the retransmit powers P_m required to achieve a given target outage probability when the number of retransmission rounds M is increased. The T_X uses the ARQ-I protocol in a Rayleigh–Rayleigh fading environment. s and R are fixed at 0.3 and 10, respectively. The results are averaged over 100,000 independent channel gain samples drawn from a uniform distribution over $[0, 1]$.

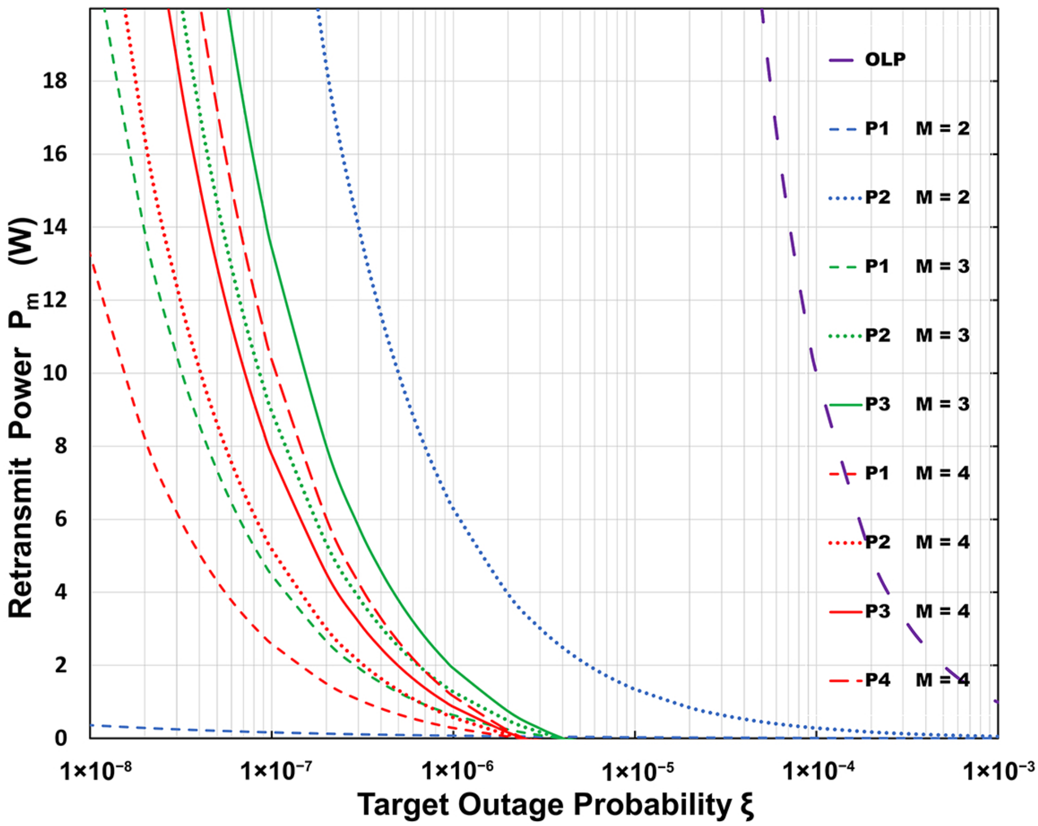

Figure 3. Retransmit power vs. target outage probability for CC-HARQ when $M = 2, 3, 4$.

This figure shows the retransmit powers P_m required to achieve a given target outage probability when the number of retransmission rounds M is increased. The T_X uses the CC-HARQ protocol in a Rayleigh–Rayleigh fading environment. s and R are fixed at 0.3 and 10, respectively. The results are averaged over 100,000 independent channel gain samples drawn from a uniform distribution over $[0, 1]$.

6.2. Variation of Retransmit Powers When the SIPR Is Varied

To show this, we make use of the special case of $M = 2$ retransmissions. Figures 4 and 5 show the variation of retransmit powers P_m with the target outage probability ξ for $M = 2$. Figure 4 corresponds to a T_X operating under the ARQ-I protocol, while Figure 5 corresponds to a T_X operating under the CC-HARQ protocol. In both figures, the retransmit powers obtained using our proposed power allocation schemes are plotted alongside the OLP values, in order to highlight the potential power savings. The simulations are conducted for three different values of the signal-to-interference protection ratio, namely $R = 5, 10$, and 15. We observe that the retransmit power levels increase with increasing values of R.

This figure shows the retransmit powers P_m required to achieve a given target outage probability. The T_X uses the ARQ-I protocol in a Rayleigh–Rayleigh fading environment. s is fixed at 0.3, while R takes values $5, 10$, and 15. The results are averaged over 100,000 independent channel gain samples drawn from a uniform distribution over $[0, 1]$.

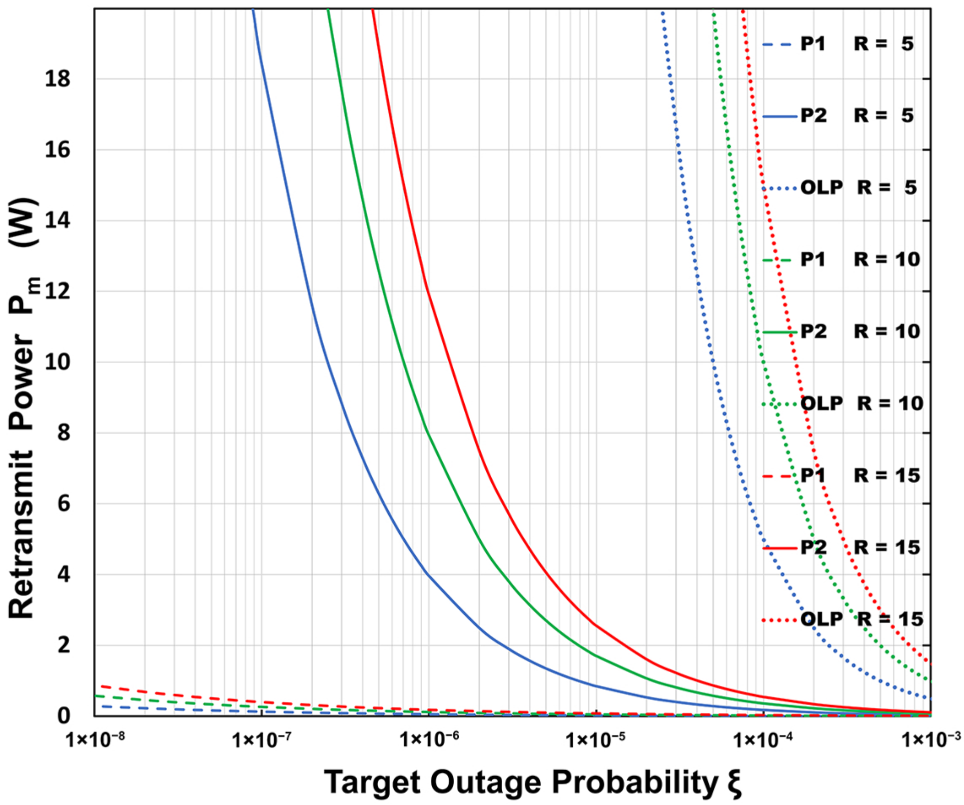

Figure 4. Retransmit power vs. target outage probability for different SIPR values for ARQ-I when $M = 2$.

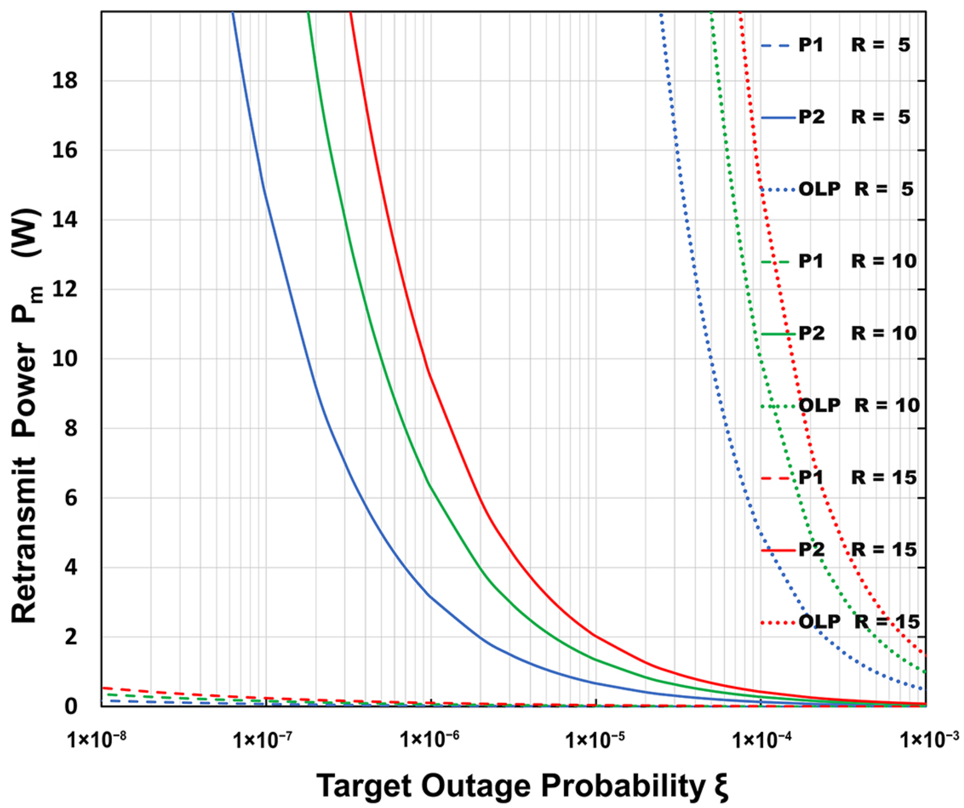

Figure 5. Retransmit power vs. target outage probability for different SIPR values for CC-HARQ when $M = 2$.

This figure shows the retransmit powers P_m required to achieve a given target outage probability. The T_X uses the CC-HARQ protocol in a Rayleigh–Rayleigh fading environment. s is fixed at 0.3, while R takes values $5, 10$, and 15. The results are averaged over 100,000 independent channel gain samples drawn from a uniform distribution over $[0, 1]$.

Although the exact quantitative rate at which retransmission power increases with SIPR cannot be expressed in simple closed form due to the non-linear outage probability formulation, the graphical results clearly demonstrate a monotonic increase in retransmission power with increasing R. Additionally, the figures confirm that allowing a greater number of retransmissions reduces the total transmit power required to satisfy the outage constraint. This reduction occurs because additional retransmission opportunities provide diversity gain, enabling the reliability target to be achieved more efficiently with lower overall power expenditure.

6.3. Normalized Power Savings of the Proposed Schemes with Respect to the OLP Values

Figure 6 shows the normalized power savings achieved when using the proposed power allocation scheme over the open-loop setup for both ARQ-I and CC-HARQ protocols for the case of two retransmissions. The plots are based on Expressions (71), (72), (88) and (89). We observe that very high power savings with respect to the open-loop setup can be obtained by using the proposed power allocation scheme. Further, we observe that the CC-HARQ scheme outperforms ARQ-I in terms of power savings. The graph is plotted only as normalized power savings vs. outage probability ξ, since the power saving expressions are independent of the signal-to-interference protection ratio R, scattered signal power of the interferer signal s, and channel gain g.

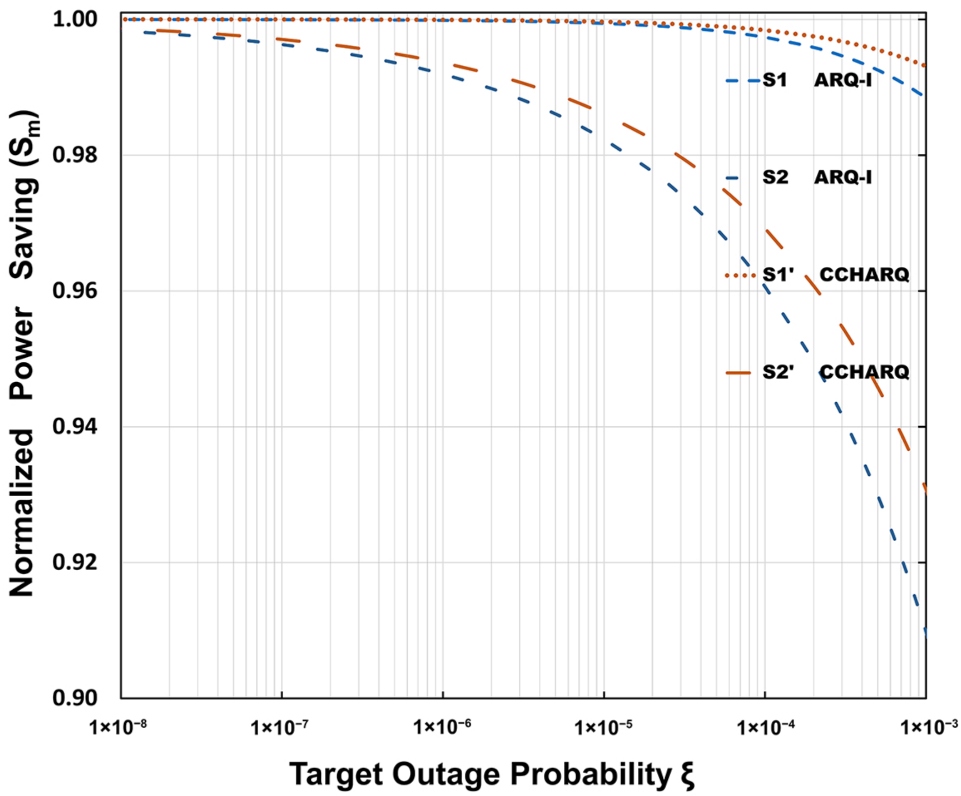

Figure 6. Normalized power savings vs. target outage probability for $M = 2$.

This figure shows the savings S_1, S_2 achieved by the ARQ-I protocol and S_1', S_2' achieved by the CC-HARQ protocol under a Rayleigh–Rayleigh fading environment. The power savings are independent of s, R, and g.

The superiority of the proposed adaptive power allocation scheme over the conventional open-loop power (OLP) approach is demonstrated both analytically and through simulation. For the case of $M = 2$, closed-form expressions for the normalized power savings relative to the OLP scheme have been derived, providing direct analytical insight into the achievable power reduction. These expressions explicitly quantify the power saving as a function of the target outage probability and system parameters. As shown in Figure 6, the analytical and simulation results consistently confirm that the proposed scheme achieves significant power savings compared to the OLP approach. This advantage becomes more pronounced in the ultra-reliable region with stringent outage probability requirements, highlighting the effectiveness of adaptive power allocation in interference-limited Rayleigh fading environments.

6.4. System Throughput

The throughput η characterizes the rate of successful message delivery over the communication channel. We proceed to find the throughput of the system by defining η as

$$\eta = \frac{K}{n}(1 - P_{out}(P_T)) \tag{91}$$

where K is the information payload in nats and n is the number of channel users. Thus, η can be obtained in nats per channel use ($npcu$) [23]. However, due to the degradation in spectral efficiency after each retransmission round, Ref. [11] proposes a modification to the throughput expression given in (91) to account for an arbitrary number of retransmissions M. Accordingly, the throughput η, without neglecting the feedback delay in channel users D, can be expressed as

$$\eta = \frac{K\left(1 - \prod_{m=1}^{M} P_{out}(P_m)\right)}{\sum_{m=1}^{M} mn \prod_{k=1}^{m-1} P_{out}(P_k) + D \sum_{m=1}^{M-1} m \prod_{k=1}^{m-1} P_{out}(P_k)}. \tag{92}$$

We plot the graph shown in Figure 7 using (92), neglecting D and assuming M was carefully chosen to avoid any delays. It is evident from this plot that the overall throughput η decreases as the number of retransmissions M increases.

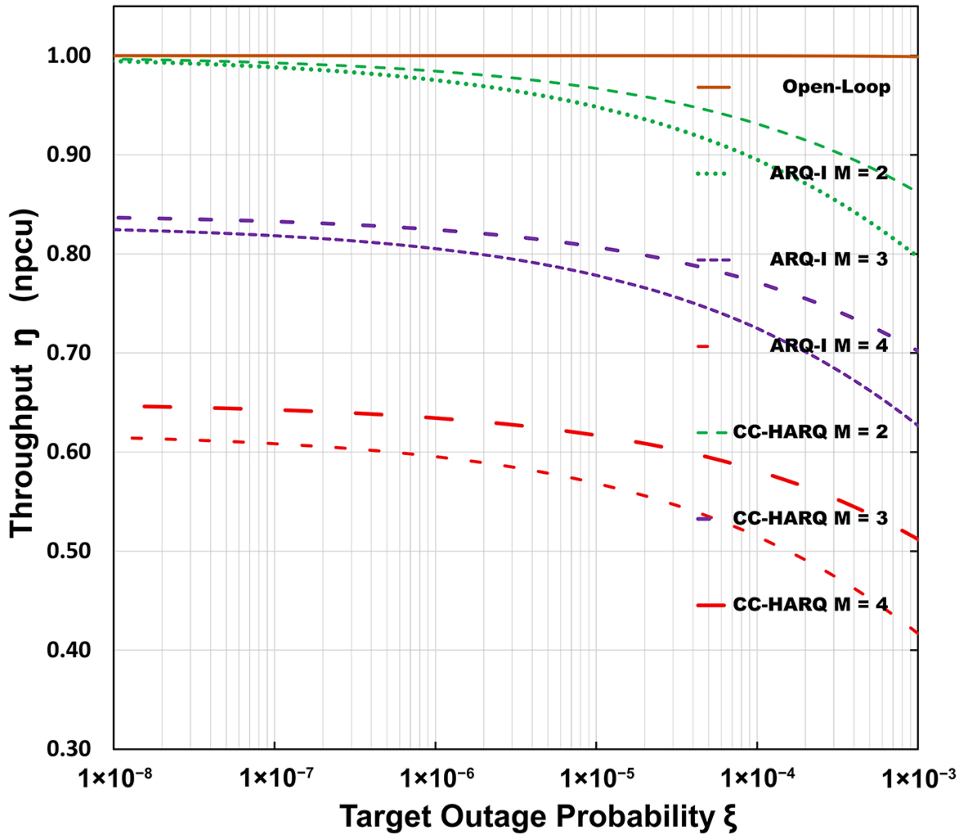

Figure 7. Throughput vs. outage probability.

The throughput η for a system communicating using ARQ-I and CC-HARQ protocols in a Rayleigh–Rayleigh fading environment, along with the outage probabilities, is plotted. $K = n = 1$ and $D = 0$. Power values are taken when $R = 10$ and $s = 0.3$. The graph has plots for $M = 2, 3$, and 4, for both protocols, along with open-loop throughput, which is $M = 1$.

6.5. Analysis of the Simulated Results

Figures 2 and 3 show that an increase in M leads to a reduction in the total power required to meet the targeted outage. However, when more retransmission rounds are allowed, each packet may undergo multiple transmission attempts before being successfully decoded, meaning each packet occupies the channel for several time slots, leading to higher end-to-end latency. At a sufficiently large M, the latency associated with it may grow beyond acceptable limits, particularly in delay-sensitive applications; thus, we cannot indefinitely increase M.

Figures 4 and 5 show that the retransmission power levels increase with increasing values of SIPR denoted by R. Since R is not the actual SIR experienced at the receiver, but rather the minimum SIR threshold that must be exceeded to avoid outage, a larger R corresponds to a more stringent reliability requirement. As R increases, the T_X must allocate higher retransmit powers to achieve the same outage target, which also explains why, in Figures 4 and 5, the curves with $R = 15$ exhibit a worse outage performance than those with $R = 10$ or $R = 5$ with the same power budget. In other words, a higher SIPR threshold makes the system more demanding and, hence, degrades performance unless compensated by larger transmit power.

Further, Figures 2 and 4 correspond to the ARQ-I protocol, while Figures 3 and 5 correspond to the CC-HARQ protocol. When comparing the retransmit power values of ARQ-I and CC-HARQ, it can be seen that the retransmit power requirements for CC-HARQ are consistently lower than those for ARQ-I. This outcome is expected, as HARQ schemes were developed as improvements to the conventional ARQ protocols. Nevertheless, this distinction serves as an implicit validation of the simulation results and the consistency of the power allocation scheme across both retransmission protocols.

Careful observation of Figures 2–5 further reveals a consistent increase in the retransmission power values across successive transmission rounds, i.e., $P_1 < P_2 < P_3 \ldots < P_M$. We prove this result for the specific case of $M = 2$ in Appendices C and E. This observation aligns well with theoretical intuition. Since the objective is to meet a predefined target outage probability ξ while spending the minimum average total power, the initial transmission is allocated a lower power. If successful, this results in significant power savings. In the event of failure, subsequent retransmissions are conducted with incrementally higher power levels, ensuring that reliability is progressively reinforced up to the maximum number of attempts M. It is also the case that optimization does not guarantee a monotonic decrease in the first transmission power P_1 as M increases. Instead, the allocation balances across all transmission rounds to minimize the expected average total power. Thus, while the trend $P_1 < P_2 < \ldots < P_M$ holds for a fixed M, comparing P_1 across different M values does not follow the same ordering. What improves consistently with increasing M is the overall outage performance and reduction in average transmit power, not necessarily each individual power level.

Figure 6 shows that the CC-HARQ scheme outperforms the ARQ-I scheme in terms of power savings. This result also agrees with intuition, since HARQ schemes were introduced as improved versions of the ARQ schemes.

Figure 7 shows that the overall throughput η decreases as the number of retransmissions M increases. This observation is consistent with the theoretical understanding of throughput, which quantifies the rate of successful message delivery over time. Although Figures 2 and 3 show that increasing M leads to a reduction in the total power required to meet a given outage probability, as explained above, it comes at the cost of increased delay. The reason is that when M is higher, many packets may require several rounds before being successfully transmitted; therefore, each packet occupies the channel for several time slots. This results in a lesser number of new packets being transmitted within a fixed time interval, thereby lowering the effective throughput.

For benchmarking, we compare our results with prior works [13,20] that studied the Rician–Rayleigh fading environment. As expected, when evaluated at the same target outage probability, both the ARQ-I scheme in [20] and the CC-HARQ scheme in [13] yield lower average retransmit power values compared to our present Rayleigh–Rayleigh case. This performance gap is mainly due to the Rician fading link, which possesses a line-of-sight path which reduces the severity of fading fluctuations compared to pure Rayleigh channels. As a result, packet reception reliability improves, which, in turn, lowers the retransmission requirement and thereby reduces the average transmit power. Between the two benchmark schemes, CC-HARQ always requires less retransmit power than ARQ-I. This relative power saving is consistent across both the Rician–Rayleigh case studied in [13] and our present Rayleigh–Rayleigh case, confirming the general power efficiency advantage of CC-HARQ over ARQ-I.

7. Conclusions and Future Work

In this work, we addressed the problem of achieving power-efficient ultra-reliable communication (URC) by minimizing the average retransmission power of a transmitter situated in a Rayleigh–Rayleigh fading environment and operating with either the ARQ-I or the CC-HARQ protocol. We derived closed-form analytical expressions for the optimal retransmit power allocation, which provide an explicit and tractable solution framework rather than relying solely on numerical optimization. Based on these expressions, we developed a sub-optimal power allocation scheme that assigns retransmit power levels across each round. Simulation results confirmed that the proposed scheme achieves significant power savings compared to the conventional open-loop power allocation. Furthermore, through benchmarking against prior works in Rician–Rayleigh fading environments, we showed that the Rayleigh–Rayleigh case serves as a conservative worst-case baseline, while the relative power-efficiency advantage of CC-HARQ over ARQ-I remains consistent across both fading models.

In addition, it was observed from the simulations that increasing the number of allowed retransmissions reduces the total power required to meet a given target outage probability. However, it was also observed through simulations that the throughput decreases with the number of retransmissions. We explained that the improvement in power efficiency comes at the cost of reduced throughput, as more retransmissions introduce additional delay and decrease the effective data rate. Consequently, the maximum number of retransmissions must be selected to balance the tradeoffs between power consumption, delay, and throughput in practical system designs.

A direct comparison with the proposed optimal adaptive allocation reveals that equal power allocation exhibits a fundamental limitation in achievable power savings, especially in the ultra-reliable regime. Since equal power allocation distributes power uniformly across retransmissions without accounting for the probabilistic structure of retransmissions, it cannot fully exploit the potential reduction in average power. In contrast, the proposed optimal allocation dynamically balances the first and second transmission powers to minimize expected consumption, resulting in significantly improved power efficiency.

https://doi.org/10.3390/telecom7050109

The proposed optimization framework can be extended to other fading models by incorporating the corresponding outage probability expressions into the optimization problem. However, the analytical tractability and availability of closed-form solutions depend strongly on the statistical properties of the underlying fading distribution. In particular, fading models such as Rician or Nakagami introduce additional mathematical complexity that may prevent closed-form solutions and require numerical optimization. Therefore, while the general optimization methodology is applicable to broader fading environments, the closed-form analytical results derived in this work are specific to the Rayleigh–Rayleigh interference-limited case and provide fundamental insights and benchmarks for more general scenarios.

For future work, we intend to extend the analysis beyond the single Rayleigh faded interferer scenario discussed in this work. Specifically, we aim to find the optimum retransmit powers when there are multiple Rayleigh interferers. Additionally, we plan to explore other fading models for the interferer, including Rician, Nakagami, and Weibull distributions, under both ARQ-I and CC-HARQ protocols. Further, we expect to find suitable convex approximations which enable the derivation of closed-form expressions for the optimal retransmit powers.

Author Contributions: Conceptualization, S.F. and U.W.; methodology, S.F., U.W. and N.D.; software, S.F. and N.D.; validation, S.F., U.W. and N.D.; formal analysis, S.F.; investigation, S.F.; resources, U.W. and N.D.; data curation, S.F. and U.W.; writing—original draft preparation, S.F.; writing—review and editing, S.F., U.W. and N.D.; visualization, S.F.; supervision, U.W. and N.D.; project administration, U.W.; funding acquisition, S.F. All authors have read and agreed to the published version of the manuscript.

Funding: This research received no external funding. Financial support for publication was provided by General Sir John Kotelawala Defence University, the institution to which the first author is affiliated.

Data Availability Statement: The original contributions presented in this study are included in the article. Further inquiries can be directed to the corresponding author.

Conflicts of Interest: The authors declare no conflicts of interest.

Appendix A. Derivation of an Expression for the Average Total Retransmit Power P_{avg}

For this purpose, let us assume that the outage probability of the m-th ARQ round is ϵ_m. Then, the probability of the Receiver R_X being unable to decode a packet after m ARQ rounds, $P_{out,m}$, will be

$$P_{out,m} = \prod_{k=1}^{m} \epsilon_k. \tag{A1}$$

Thus, the probability of the Receiver R_X being able to decode a packet after m ARQ rounds, $P_{suc,m}$, can be found by

$$P_{suc,m} = P_{out,m-1} - P_{out,m}. \tag{A2}$$

Note that $P_{out,0}$ prompted from the above expression gives the probability of the Receiver R_X being unable to decode a packet when no retransmission rounds are initiated, and this is clearly unity.

Further, let us assume that the retransmit power of the m-th ARQ round is P_m. Then, the total retransmit power up to m-th ARQ round,

$$P_{total,m} = \sum_{k=1}^{m} P_k. \tag{A3}$$

Thus, the average total retransmit power P_{avg}, can be obtained by

$$P_{avg} = \sum_{m=1}^{M-1} [P_{suc,m}\, P_{total,m}] + (P_{out,M-1}\, P_{total,M}). \tag{A4}$$

Simplifying this expression by using (A2) and changing the order of summation,

$$\begin{aligned}
&P_{avg} \\
&= \sum_{m=1}^{M-1} \sum_{k=1}^{m} (P_{out,m-1} - P_{out,m}) P_k + \sum_{k=1}^{M} P_{out,M-1} P_k \\
&= \sum_{k=1}^{M} \sum_{m=k}^{M-1} (P_{out,m-1} - P_{out,m}) P_k + \sum_{k=1}^{M} P_k P_{out,M-1} \\
&= \sum_{k=1}^{M} P_k \begin{bmatrix} P_{out,k-1} & - P_{out,k} & \\ + P_{out,k} & - P_{out,k+1} & \\ + P_{out,k+1} & - P_{out,k+2} & + P_{out,M-1} \\ & \vdots & \\ + P_{out,M-2} & - P_{out,M-1} & \end{bmatrix} \\
&= \sum_{k=1}^{M} P_k P_{out,k-1}.
\end{aligned} \tag{A5}$$

Therefore, the average retransmit power P_{avg} of a T_X that uses the ARQ principle would be

$$P_{avg} = \sum_{k=1}^{M} P_m P_{out,m-1},$$

which is the expression used in (9).

Appendix B. Proof of Non-Convexity

The objective functions of the optimization problems in (15) and (16) can be written for the $M = 2$ case as the following single expression.

$$P_1 + P_2 \left(\frac{w}{w + P_1} \right), \tag{A6}$$

This expression is also obtained in (59) and (78).

A second-order Hessian Matrix H for P_{avg} is in the form $H = \begin{bmatrix} \frac{\partial^2 P_{avg}}{\partial {P_1}^2} & \frac{\partial^2 P_{avg}}{\partial P_1 \partial P_2} \\ \frac{\partial^2 P_{avg}}{\partial P_2 \partial P_1} & \frac{\partial^2 P_{avg}}{\partial {P_2}^2} \end{bmatrix}$, and by plugging in the expressions for the partial derivatives, we get

$$H = \begin{bmatrix} \frac{2wP_2}{(w+P_1)^3} & -\frac{w}{(w+P_1)^2} \\ -\frac{w}{(w+P_1)^2} & 0 \end{bmatrix}. \tag{A7}$$

We can observe that this H is real since $w = \frac{Rs}{g} > 0$ and $P_1, P_2 > 0$. It is also symmetric. In such cases, for the function under consideration to be convex, $x^T H x > 0$, where $x = [x_1 \quad x_2]^T \in \mathbb{R}^2$ [38]. Thus, we compute $x^T H x$ as

$$\begin{aligned}
&x^T H x \\
&= \begin{bmatrix} x_1 & x_2 \end{bmatrix} \begin{bmatrix} \frac{2wP_2}{(w+P_1)^3} & -\frac{w}{(w+P_1)^2} \\ -\frac{w}{(w+P_1)^2} & 0 \end{bmatrix} \begin{bmatrix} x_1 \\ x_2 \end{bmatrix} \\
&= \frac{2wP_2 {x_1}^2}{(w + P_1)^3} - \frac{2w x_1 x_2}{(w + P_1)^2} \\
&= \frac{2wP_2}{(w + P_1)^3} \left[\left(x_1 - \frac{(w + P_1) x_2}{2P_2} \right)^2 - \frac{(w + P_1)^2 {x_2}^2}{4{P_2}^2} \right].
\end{aligned} \tag{A8}$$

We could observe the following.

- $x_1 = x_2 = 0 \Rightarrow x^T M x = 0$.
- $x_1 \neq 0, x_2 = 0 \Rightarrow x^T M x = \frac{2wP_2}{(w+P_1)^3} {x_1}^2 > 0$.
- If chosen x_2 such that $\frac{(w+P_1)}{2P_2} x_2 = k$ and $0 < x_1 < k \Rightarrow x^T M x < 0$.

From these, we understand that $x^T M x$ can be positive, negative or zero [39]. Thus, we conclude that the given objective function is non-convex.

Appendix C. Proving $P_2 > P_1$ for ARQ-I

Here, we will prove that P_2 will always be greater than P_1 for the particular case of $M = 2$ for the ARQ-I protocol.

We consider $P_2 - P_1$ as follows.

$$\begin{aligned} &P_2 - P_1 \\ &= wA + \frac{wA^2}{2} - wA \\ &= \frac{wA^2}{2} \end{aligned} \tag{A9}$$

Now, from (8), it is evident that $w > 0$. Also, since χ is in the required range, as shown in Section 5.1.4, we get $A > 0$. Therefore, $P_2 - P_1 > 0 \Rightarrow P_2 > P_1$.

Appendix D. Proving That the Lower Bound of χ' is in the Acceptable Range

For $(P_1)_0$ to be positive, χ' should be greater than $\frac{3+\sqrt{15}}{6}$. However, since χ' is a function of the target outage probability ξ according to (83), χ' is automatically bound by the range of ξ. Therefore, $0 \leq \xi \leq 1 \Rightarrow \sqrt[3]{\frac{3}{4} + \frac{1}{4}\sqrt{9 + \frac{2}{27}}} \leq \chi' < \infty$.

However, $\sqrt[3]{\frac{3}{4} + \frac{1}{4}\sqrt{9 + \frac{2}{27}}}$ can be simplified as follows.

$$\begin{aligned} &\sqrt[3]{\frac{3}{4} + \frac{1}{4}\sqrt{9 + \frac{2}{27}}} \\ &= \sqrt[3]{\frac{3}{4} + \frac{1}{4}\sqrt{\frac{49 \times 5}{9 \times 3}}} \\ &= \sqrt[3]{\frac{3}{4} + \frac{7\sqrt{15}}{36}} \\ &= \sqrt[3]{\frac{162 + 42\sqrt{15}}{216}} \\ &= \sqrt[3]{\frac{3^3 + 3 \cdot 3^2 \cdot \sqrt{15} + 3 \cdot 3 \cdot \sqrt{15}^2 + \sqrt{15}^3}{216}} \\ &= \sqrt[3]{\frac{\left(3 + \sqrt{15}\right)^3}{6^3}} \\ &= \frac{3 + \sqrt{15}}{6}. \end{aligned} \tag{A10}$$

Thus, it is evident that $\sqrt[3]{\frac{3}{4} + \frac{1}{4}\sqrt{9 + \frac{2}{27}}} \leq \chi' < \infty$ is the same as $\frac{3+\sqrt{15}}{6} \leq \chi' < \infty$, which is the required range for the $(P_1)_0$ to be positive.

Appendix E. Proving $P_2 > P_1$ for CC-HARQ

Here, we show that P_2 will always be greater than P_1 for the particular case of $M = 2$ for the CC-HARQ protocol.

As in Appendix C, we consider $P_2 - P_1$.

$$\begin{aligned} &P_2 - P_1 \\ &= \frac{w}{2}\left(1 + 4A' + 2A'^2\right) - wA' \\ &= \frac{w}{2}\left(1 + 2A' + 2A'^2\right) \end{aligned} \tag{A11}$$

Now, from (8), it is evident that $w > 0$. Also, since χ' is in the required range, as shown in Section 5.2.4, we get $A' > 0$. Therefore, $P_2 - P_1 > 0 \Rightarrow P_2 > P_1$.

References

1. Proakis, J.G.; Salehi, M. *Digital Communications*, 4th ed.; McGraw-Hill: New York, NY, USA, 2000.
2. Rappaport, T.S. *Wireless Communications: Principles and Practice*, 2nd ed.; Prentice Hall PTR: Upper Saddle River, NJ, USA, 2002.
3. Karagiannidis, G.; Kotsopoulos, S.; Georgopoulos, C. Outage probability analysis for a Rician signal in L Nakagami interferers with arbitrary parameters. *J. Commun. Netw.* **1999**, *1*, 26–30. [CrossRef]
4. Tullberg, H.; Popovski, P.; Li, Z.; Uusitalo, M.A.; Hoglund, A.; Bulakci, O.; Fallgren, M.; Monserrat, J.F. The METIS 5G system concept: Meeting the 5G requirements. *IEEE Commun. Mag.* **2016**, *54*, 132–139. [CrossRef]
5. She, C.; Dong, R.; Gu, Z.; Hou, Z.; Li, Y.; Hardjawana, W.; Yang, C.; Song, L.; Vucetic, B. Deep learning for ultra-reliable and low-latency communications in 6G networks. *IEEE Netw.* **2020**, *34*, 219–225. [CrossRef]
6. Hossain, A.; Pan, Z.; Saito, M.; Liu, J.; Shimamoto, S. Multiband massive channel random access in ultra-reliable low-latency communication. *IEEE Access* **2020**, *8*, 81492–81505. [CrossRef]
7. Verma, S.; Kaur, S.; Khan, M.A.; Sehdev, P.S. Towards green communication in 6G-enabled massive Internet of Things. *IEEE Internet Things J.* **2020**, *8*, 5408–5415. [CrossRef]
8. Palattella, M.R.; Dohler, M.; Grieco, A.; Rizzo, G.; Torsner, J.; Engel, T.; Ladid, L. Internet of Things in the 5G era: Enablers, architecture, and business models. *IEEE J. Sel. Areas Commun.* **2016**, *34*, 510–527. [CrossRef]
9. Andreev, S.; Galinina, O.; Pyattaev, A.; Gerasimenko, M.; Tirronen, T.; Torsner, J.; Sach, J.; Dohler, M.; Koucheryavy, Y. Understanding the IoT connectivity landscape: A contemporary M2M radio technology roadmap. *IEEE Commun. Mag.* **2015**, *53*, 32–40. [CrossRef]
10. Ayaz, M.; Ammad-Uddin, M.; Sharif, Z.; Mansour, A.; Aggoune, E.-H.M. Internet-of-Things (IoT)-based smart agriculture: Toward making the fields talk. *IEEE Access* **2019**, *7*, 129551–129583. [CrossRef]
11. Dosti, E.; Wijewardhana, U.L.; Alves, H.; Latva-aho, M. Ultra reliable communication via optimum power allocation for Type-I ARQ in finite block-length. In *Proceedings of the 2017 IEEE International Conference on Communications (ICC), Paris, France, 21–25 May 2017*; IEEE: Piscataway, NJ, USA, 2017; pp. 1–6.
12. Dosti, E.; Shehab, M.; Alves, H.; Latva-Aho, M. Ultra reliable communication via optimum power allocation for HARQ retransmission schemes. *IEEE Access* **2020**, *8*, 89768–89781. [CrossRef]
13. Fernando, S.; Wijewardhana, U.; Dharmaweera, N. Power efficient ultra-reliable communication in Rician/Rayleigh fading environment using CC-HARQ. In *Proceedings of the 2023 Moratuwa Engineering Research Conference (MERCon), Moratuwa, Sri Lanka, 9–11 November 2023*; IEEE: Piscataway, NJ, USA, 2023; pp. 450–455.
14. Dosti, E.; Shehab, M.; Alves, H.; Latva-aho, M. Ultra reliable communication via CC-HARQ in finite block-length. In *Proceedings of the 2017 European Conference on Networks and Communications (EuCNC), Oulu, Finland, 12–15 June 2017*; IEEE: Piscataway, NJ, USA, 2017; pp. 1–5.
15. Praneeth, V.V.K.; Mansour, N.; Dahlhaus, D. Chase Combining Hybrid ARQ Type II cross-layer optimization for underlay cognitive radio. In Proceedings of the 2024 IEEE Wireless Communications and Networking Conference (WCNC), Dubai, United Arab Emirates, 21–24 April 2024; pp. 1–7.
16. Comroe, R.; Costello, D. ARQ schemes for data transmission in mobile radio systems. *IEEE J. Sel. Areas Commun.* **1984**, *2*, 472–481. [CrossRef]
17. Chih-Lin, I.; Rowell, C.; Han, S.; Xu, Z.; Li, G.; Pan, Z. Toward green and soft: A 5G perspective. *IEEE Commun. Mag.* **2014**, *52*, 66–73. [CrossRef]
18. Fernando, S.; Wijewardhana, U.; Dharmaweera, N. Power efficient ultra-reliable communication for Rayleigh faded IR-HARQ systems. In *Proceedings of the 2023 Moratuwa Engineering Research Conference (MERCon), Moratuwa, Sri Lanka, 9–11 November 2023*; IEEE: Piscataway, NJ, USA, 2023; pp. 456–461.

19. Makki, B.; Svensson, T.; Zorzi, M. Green communication via Type-I ARQ: Finite block-length analysis. In *Proceedings of the 2014 IEEE Global Communications Conference, Austin, TX, USA, 8–12 December 2014*; IEEE: Piscataway, NJ, USA, 2014; pp. 2673–2677.
20. Fernando, S.; Wijewardhana, U.; Dharmaweera, N. Ultra reliable communication in Rician/Rayleigh fading environment using Type-I ARQ. In *Proceedings of the 2021 10th International Conference on Information and Automation for Sustainability (ICIAfS), Negambo, Sri Lanka, 11–13 August 2021*; IEEE: Piscataway, NJ, USA, 2021; pp. 209–213.
21. Gao, Y.; Yang, T.; Hu, B. Improving the transmission reliability in smart factory through spatial diversity with ARQ. In *Proceedings of the 2016 IEEE/CIC International Conference on Communications in China (ICCC), Chengdu, China, 27–29 July 2016*; IEEE: Piscataway, NJ, USA, 2016; pp. 1–5.
22. Shehab, M.; Alves, H.; Latva-aho, M. Ultra reliable communication via opportunistic ARQ transmission in cognitive networks. In *Proceedings of the 2018 IEEE Wireless Communications and Networking Conference (WCNC), Barcelona, Spain, 15–18 April 2018*; IEEE: Piscataway, NJ, USA, 2018; pp. 1–6.
23. Devassy, R.; Durisi, G.; Popovski, P.; Ström, E.G. Finite-blocklength analysis of the ARQ-protocol throughput over the Gaussian collision channel. In Proceedings of the 2014 6th International Symposium on Communications, Control and Signal Processing (ISCCSP), Athens, Greece, 21–23 May 2014; pp. 173–177.
24. Chaitanya, T.V.K.; Le-Ngoc, T. Energy-efficient adaptive power allocation for Incremental MIMO systems. *IEEE Trans. Veh. Technol.* **2016**, *65*, 2820–2827. [CrossRef]
25. Chaitanya, T.V.K.; Larsson, E.G. Optimal power allocation for Hybrid ARQ with Chase Combining in i.i.d. Rayleigh fading channels. *IEEE Trans. Commun.* **2013**, *61*, 1835–1846. [CrossRef]
26. Wahid, A.; Zain, S.; Imtiaz, N.; Muhammad, M.; Alharbi, A.; Tolba, A.; Al-Khasawneh, M.; Ullah, I. Enhancing Security with Hybrid Active-Passive RIS: A DRL Approach Against Eavesdropping and Jamming. *IEEE Access* **2025**, *13*, 3632–3643. [CrossRef]
27. Bian, F. Lightweight Convolutional Neural Network for Multiscale Temporal Modeling in Ultra-Reliable Low-Latency Communication. In Proceedings of the 2025 4th International Symposium on Computer Applications and Information Technology (ISCAIT), Xi'an, China, 21–23 March 2025; pp. 1364–1368.
28. Saravanan, N.; Lakshmi, G.J. Revolutionizing Connectivity: Unveiling Next-Gen Efficiency with 6G's Ultra-Reliable Low Latency Communications Resource Allocation. In Proceedings of the 2024 First International Conference on Pioneering Developments in Computer Science and Digital Technologies (IC2SDT), Delhi, India, 2–4 August 2024; pp. 451–455.
29. Chong, B.; Lu, H.; Cheng, G. Exploiting Semantic Communications for Ultra-Reliable Low-Latency Communications. *IEEE Trans. Commun.* **2025**, *73*, 11340–11354. [CrossRef]
30. Mohammad, R.; Mozayani, N. Using Machine Learning Algorithms in Edge Intelligence for Ultra-Reliable and Low-Latency Communications in the Industrial Metaverse. In Proceedings of the 2025 29th International Computer Conference, Computer Society of Iran (CSICC), Tehran, Iran, 5–6 February 2025; pp. 1–5.
31. Xin, Y.; Wang, X.; Leus, G.; Yue, G.; Jiang, J. Interference management in wireless communication systems: Theory and applications. *Eurasip J. Wirel. Commun. Netw.* **2011**, *2010*, 687649. [CrossRef]
32. Shah, A.; Haimovich, A. Performance analysis of optimum combining in wireless communications with Rayleigh fading and cochannel interference. *IEEE Trans. Commun.* **1998**, *46*, 473–479. [CrossRef]
33. Goldsmith, A. *Wireless Communications*; Cambridge University Press: Cambridge, UK, 2005.
34. Cardieri, P. Modeling Interference in Wireless Ad Hoc Networks. *IEEE Commun. Surv. Tutor.* **2010**, *12*, 551–572. [CrossRef]
35. Haug, J.; Ucci, D. Microcellular radio performance in a Rayleigh/Rician cochannel interference environment. In Proceedings of the 1st International Conference on Universal Personal Communications—ICUPC '92 Proceedings, Dallas, TX, USA, 29 September–1 October 1992; pp. 04.06/1–04.06/4.
36. Tjhung, T.T.; Chai, C.C.; Dong, X. Outage probability for a Rician signal in L Rician interferers. *Electron. Lett.* **1995**, *31*, 532–533. [CrossRef]
37. Polyanskiy, Y.; Poor, V.; Verdu, S. Channel Coding Rate in the Finite Blocklength Regime. *IEEE Trans. Inf. Theory* **2010**, *56*, 2307–2359. [CrossRef]
38. Boyd, S.; Vandenberghe, L. *Convex Optimization*, 1st ed.; Cambridge University Press: Cambridge, UK, 2004.
39. Bertsekas, D.P. *Nonlinear Programming*, 3rd ed.; Athena Scientific: Boston, MA, USA, 2016.
40. Abramowitz, M.J.; Stegun, I.A. (Eds.) *Handbook of Mathematical Functions: With Formulas, Graphs, and Mathematical Tables*, 9th ed.; Dover Publications: Garden City, NY, USA, 1965.
41. Cormen, T.H.; Leiserson, C.E.; Rivest, R.L.; Stein, C. *Introduction to Algorithms*, 4th ed.; The MIT Press: Cambridge, MA, USA, 2022.